ORNL-3556
UC-25 – Metals, Ceramics, and Materials
TID-4500 (29th ed.)

THERMAL CONDUCTIVITY OF URANIUM DIOXIDE AND ARMCO IRON BY AN IMPROVED RADIAL HEAT FLOW TECHNIQUE

T. G. Godfrey
W. Fulkerson
T. G. Kollie
J. P. Moore
D. L. McElroy

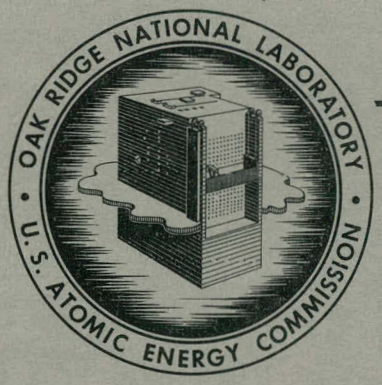

OAK RIDGE NATIONAL LABORATORY
operated by
UNION CARBIDE CORPORATION
for the
U.S. ATOMIC ENERGY COMMISSION

DISCLAIMER

Printed in USA. Price: $1.75 Available from the
Office of Technical Services
U. S. Department of Commerce
Washington 25, D. C.

ORNL-3556

Contract No. W-7405-eng-26

METALS AND CERAMICS DIVISION

THERMAL CONDUCTIVITY OF URANIUM DIOXIDE AND ARMCO IRON BY AN IMPROVED RADIAL HEAT FLOW TECHNIQUE

T. G. Godfrey
W. Fulkerson
T. G. Kollie
J. P. Moore
D. L. McElroy

JUNE 1964

OAK RIDGE NATIONAL LABORATORY
Oak Ridge, Tennessee
operated by
UNION CARBIDE CORPORATION
for the
U. S. ATOMIC ENERGY COMMISSION

THIS PAGE

WAS INTENTIONALLY

LEFT BLANK

CONTENTS

LIST OF SYMBOLS

A See Eq. 4, cm °K w^{-1}

A^* Cross-sectional area, cm^2

a A constant defined by Eq. 16, w cm^{-1} $°K^{-1}$

B See Eq. 4, cm/w

b A constant defined by Eq. 16, unitless

C_V Heat capacity at constant volume, wsec $°K^{-1}$ $g\text{-}mole^{-1}$

C_P Heat capacity at constant pressure, wsec $°K^{-1}$ $g\text{-}mole^{-1}$

C_1 A constant defined by Eq. 27, μohm-cm

C_2 A constant defined by Eq. 27, μohm-cm/°K

C_3 A constant defined by Eq. 27, μohm-cm/$°K^3$

c_V Specific heat at constant volume, wsec $°K^{-1}$ cm^{-3}

c_P Specific heat at constant pressure w sec $°K^{-1}$ g^{-1}

E Modulus of elasticity, dynes/cm^2

E_G Forbidden band gap, ev

e Electronic charge, coulombs

h Planck's constant, 6.628×10^{-34} $wsec^2$

$\bar{I}$ Average electric current, amp

k Total thermal conductivity, w cm^{-1} $°K^{-1}$

k_u Reciprocal of R_u, the thermal resistance due to umklapp processes, w cm^{-1} $°K^{-1}$

k_0 See Eq. 17, w cm^{-1} $°K^{-1}$

k_L Lattice portion of the thermal conductivity, w cm^{-1} $°K^{-1}$

k_e Electronic portion of the thermal conductivity, w cm^{-1} $°K^{-1}$

k Boltzmann's constant, 1.38×10^{-23}, wsec/°K

L Theoretical value of the Wiedemann-Franz-Lorenz constant, 2.45×10^{-8} w-ohm/$°K^2$

L^* Length between voltage taps, cm

$\bar{\ell}_i$ Average phonon mean free path, cm

$\bar{\ell}_u$ Average phonon mean free path due to umklapp processes, cm

$\bar{\ell}_I$ Average phonon mean free path due to phonon impurity interaction, cm

M Mass per atom, g

N_i Concentration of impurities of type "i," number/cm^3

n A constant in Eq. 16, unitless

Q Heat flow rate, w

R Thermal resistance, cm °K w^{-1}

R_u Thermal resistance due to umklapp processes, cm °K w^{-1}

R_I Thermal resistance due to impurity scattering, cm °K w^{-1}

r Radial position in a specimen relative to the cylindrical axis, cm

r_1 Radial position of inside thermocouples, cm

r_2 Radial position of the outside thermocouples, cm

S Seebeck coefficient, μv/°K

T Absolute temperature, °K

t Temperature, °C

V Molar volume, cm^3/g-mole

$\bar{V}_1$ Average thermocouple emf of thermocouples at radius r_1

$\bar{V}_2$ Average thermocouple emf of thermocouples at radius r_2

$\bar{v}$ Average phonon velocity, cm/sec

α Thermal diffusivity, cm^2/sec

α_v Volume thermal expansion coefficient, $°K^{-1}$

α_L Linear thermal expansion coefficient, $°K^{-1}$

Δ A symbol representing a finite change

δ Cube root of the volume per atom, cm

ϵ Determinable error, unitless

γ Gruneisen constant defined by Eq. 11, unitless

κ Isothermal compressibility, cm^3/ wsec

π 3.1416

ρ Electrical resistivity, μohm-cm

ρ_0 A constant defined by Eq. 31, μohm-cm

ρ^* Density, g/cm^3

σ Electrical conductivity, μohm-cm^{-1}

σ_e The portion of the electrical conductivity due to electrons, μohm-cm^{-1}

σ_h The portion of the electrical conductivity due to holes, μohm-cm^{-1}

σ_i Scattering cross section of "i" type impurity, cm^2

θ_D Debye temperature, °K

Ω Electrical resistance, ohms

THERMAL CONDUCTIVITY OF URANIUM DIOXIDE AND ARMCO IRON BY AN IMPROVED RADIAL HEAT FLOW TECHNIQUE

T. G. Godfrey, W. Fulkerson, T. G. Kollie, J. P. Moore, and D. L. McElroy

ABSTRACT

A description of an improved radial heat flow technique for measuring the thermal conductivity of solids in the range −57 to 1100°C is presented. The technique yielded results with a probable accuracy of ±1.5% and a reproducibility of ±0.1% in this range. Meaningful measurements were limited to 1100°C by Pt vs Pt–10% Rh thermocouple instability, although the apparatus was structurally sound to 1400°C. The thermal conductivity of polycrystalline UO_2 was measured from −57 to 1100°C and reveals a maximum in k near room temperature caused by the decrease of the lattice specific heat. The thermal resistance, $1/k$, shows a linear dependence with temperature from 200 to 1000°C, which is expected for an insulator well above its Debye temperature. The slope of the $1/k$-temperature plot is 0.0223 cm/w, and this is independent of impurity content, although the intercept is sensitive to impurity content. The thermal conductivity of polycrystalline Armco iron was measured between 100 and 1000°C and was found to be within ±2 to 3% of the best values reported in the literature. The temperature dependence of the thermal conductivity of iron is largely controlled by the electronic contribution, which was deduced from electrical conductivity measurements. The thermal conductivity of iron can be represented by four linear equations for the temperature ranges 0 to 436, 436 to 786, 786 to 910, and 910 to 1000°C. A slope change of 30% at 436°C may be coupled to a minimum in the thermoelectric power of iron near this temperature. A minimum in the thermal conductivity occurs near 786°C and is associated with the Curie transformation. A 4% decrease in the thermal conductivity was observed at the α-γ transformation (910°C), and this is associated with a change in the lattice contribution to the total thermal conductivity.

INTRODUCTION

The first objective of this work was to develop apparatuses and techniques capable of producing very accurate thermal conductivity values for solid specimens between room temperature and 1400°C. A second goal was to study materials of nuclear and scientific interest to learn about the heat-transfer mechanisms controlling thermal conductivity, k.

There is no universal thermal conductivity method which is applicable for use for all solid specimens at all temperatures. For this reason a number of overlapping methods are necessary to measure k over a wide spectrum of specimens and temperatures. The radial heat flow apparatus described here is one such method which Powell[1] developed in 1939 to measure k of Armco iron. It is an absolute method and is capable of very good accuracy. For this reason

[1] R. W. Powell, "Further Measurements of the Thermal and Electrical Conductivity of Iron at High Temperatures," *Proc. Phys. Soc. (London)* 51, 407 (1939).

the present apparatus was developed to measure materials which can be used as standards in checking the accuracy of other methods under development. The method has disadvantages in that large specimens are required and that measurements at a given temperature normally require 8 hours.

The versatility and accuracy of the radial heat flow apparatus were demonstrated by measurements on two widely different materials, UO_2 and Armco iron. Uranium dioxide is a semiconductor with a low thermal conductivity, whereas iron is a metal with a high thermal conductivity. Both of these materials have been measured extensively by other investigators and thus afford ample grounds for comparison. However, accurate measurements of the thermal conductivity of both materials are of scientific interest to enable the differentiation of the various heat transfer mechanisms operative in these two materials. In fact, there is a heated debate[2-7] about whether or not k of UO_2 reactor fuel elements increases at very high temperatures and about what mechanisms could cause such an increase. The debate can be settled only by good high-temperature measurements. In addition, recent data taken below room temperature by Béthoux, Thomas, and Weil[8] show that k of UO_2 has two local maxima – one at about 300°K and another at about 10°K. This shape of the thermal conductivity–temperature curve is related to the antiferromagnetic-paramagnetic transition at about 30°K (ref 8). This effect was also verified qualitatively by a group at CEN.[9] In light of this information, a much closer scrutiny of the thermal conductivity of UO_2 at room temperature and below was in order.

Armco iron is considered by many to be a thermal conductivity standard, and Powell[10] recently reviewed the published data. This review shows that below 600°C the data spread is about 4% but becomes progressively larger at higher temperatures, amounting to 42% at 900°C. Because of the spread, more accurate high-temperature measurements are needed. In addition, there is considerable uncertainty about the effect of the ferromagnetic-paramagnetic transition and the α-γ phase transformation on the thermal conductivity so that additional measurements at these temperatures are of interest.

---

[2]J. L. Bates, "Thermal Conductivity of UO_2 Improves at High Temperature," *Nucleonics* 19(6), 83 (1961).

[3]D. Wiedenbaum, *High Performance UO_2 Program – Quarterly Progress Report No. 8, January–March 1963*, GEAP-3771-8 (Apr. 15, 1963), sec 4, pp 10–11.

[4]J. A. L. Robertson *et al.*, "Temperature Distribution in UO_2 Fuel Elements," *J. Nucl. Mater.* 7(3), 248–54 (1962).

[5]I. Cohen, B. Lustman, and J. E. Eichenberg, *Measurement of the Thermal Conductivity of Metal-Clad Uranium Oxide Rods During Irradiation*, WAPD-228 (August 1960).

[6]A. J. Anthony, C. E. Burdg, and R. J. Sanderson, "Out-of-Pile Thermal Testing of UO_2 Fuel Elements," *Trans. Am. Nucl. Soc.* 5(1), 236 (1962).

[7]M. F. Lyons *et al.*, "UO_2 Thermal Conductivity at Elevated Temperatures," *Trans. Am. Nucl. Soc.* 6(1), 152 (1963).

[8]O. Béthoux, P. Thomas, and L. Weil, "Conductibilite thermique de UO_2 a basse temperature," *Compt. Rend.* 253(19), 2043–45 (1961).

[9]*Minutes of Ceramic Fuels Meeting Held in Brussels, 3–5 Oct., 1962*, Euratom–United States Joint Research and Development Board, TID-7666 and EUR/C/4936 62e, p 20.

[10]R. W. Powell, "Armco Iron as a Thermal Conductivity Standard. Part I, Review of Published Data," p 454 in *Progress in International Research on Thermodynamic and Transport Properties* (ed. by Joseph F. Mesi and Donald H. Tsai), The American Society of Mechanical Engineers and Academic Press, New York, 1962.

For iron, much of the heat is transported by electrons, so measurements of electrical conductivity are helpful in evaluating thermal conductivity behavior. Therefore supplementary electrical conductivity measurements were made on this material.

The following sections contain extensive descriptions of the experimental apparatus and techniques as well as a detailed characterization of the specimens tested. These were included to allow critical evaluation of this work.

DESCRIPTION OF THE APPARATUS

The present radial heat flow apparatus was designed to produce a measurable outward radial heat flow in a cylindrical specimen consisting of a stack of disks, several of which are instrumented with thermocouples to determine the radial temperature gradient. Each specimen disk had a central $\frac{5}{8}$-in. hole, and the heat flow was generated by an axial core heater carefully positioned in this hole. The overall temperature of the specimen was maintained by an enclosing cylindrical

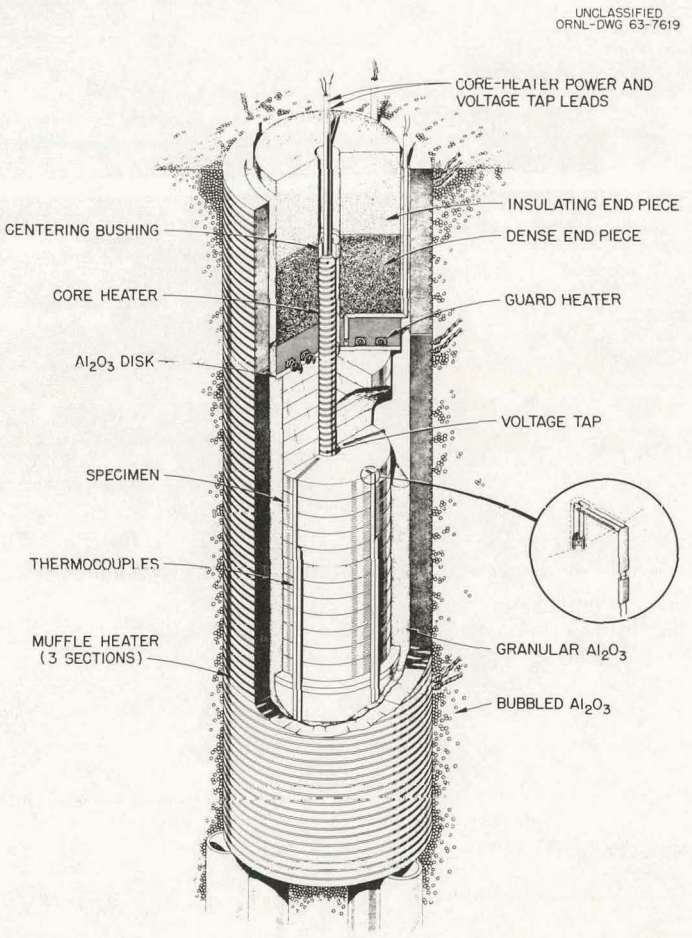

Fig. 1. Schematic Drawing of Apparatus.

muffle heater. Radial heat flow was ensured by the use of end guard heaters and also by adjusting the power to the separately wound end sections of the muffle heater. To protect the specimen from oxidation, the apparatus was contained in a water-cooled brass chamber under 1 atm of helium which was 99.999% pure. To prevent convection currents and to minimize radiation losses, the annuli between the specimen and the muffle heater and between the specimen and the core heater were filled with granular alumina. For thermal insulation the space outside the muffle heater was filled with bubbled alumina. Figure 1 is a schematic drawing of the apparatus. Figures 2(*a*) and 2(*b*) show the apparatus in stages of assembly.

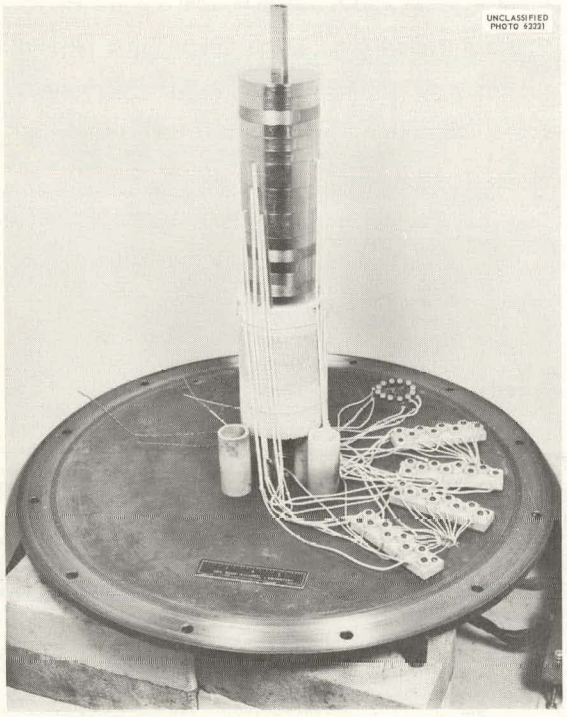

Fig. 2(*a*). Armco Iron Specimen Disks in the Radial Heat Flow Apparatus, Showing the Thermocouples, the Bottom Guard Heater, the Bottom Insulating Pieces, and the Thermocouple Connection Blocks. The brass axial rod is an assembly aid.

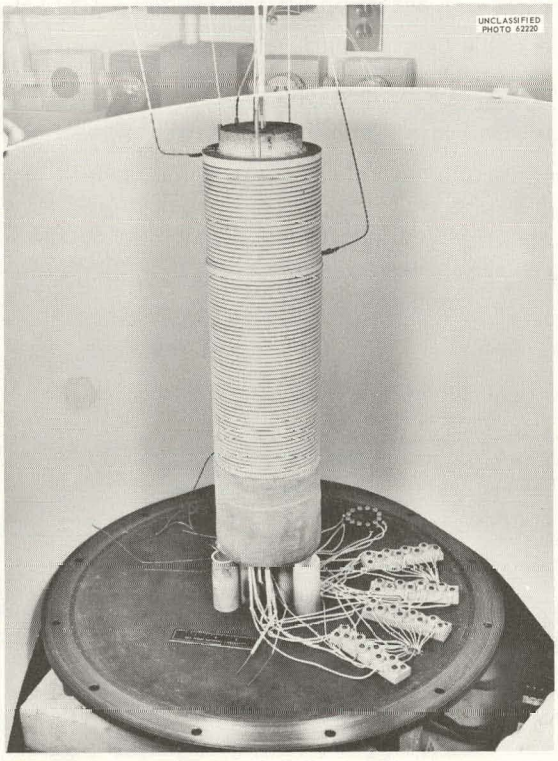

Fig. 2(*b*). Radial Heat Flow Apparatus, Showing the Three Independent Sections of the Muffle Heater in Place.

Core Heater

The core heater was made by winding a double strand of 0.020-in.-diam Pt–10% Rh wire on a $\frac{3}{8}$-in.-OD, 15-in.-long Coors AD-99 alumina tube grooved 9 turns per inch. Two small holes were drilled exactly 3 in. apart in the center section of the tube. These holes accommodated the 0.020-in. Pt–10% Rh voltage taps which were tweezer-welded to both heater wires. The voltage taps

and the input power leads were connected to 12-gage copper wires just inside the water-cooled brass shell. These and all other power leads passed through the shell by means of large Kovar seals.

Muffle and Guard Heaters

The muffle assembly consisted of a 10-in. center section and two 5-in. end sections, as shown in Fig. 2. Each section consisted of a 5-in.-OD × 4-in.-ID McDaniel high-purity alumina tube which was grooved 5 turns per inch to accommodate a bifilar winding of 0.047-in.-diam molybdenum wire. The end guard heaters were 1-in.-thick $3\frac{1}{2}$-in.-OD spirally grooved alumina disks. A coiled winding of 0.040-in.-diam molybdenum wire was cemented into the spiral groove with alumina cement. A $\frac{1}{8}$-in.-thick $3\frac{1}{2}$-in.-OD Coors AD-99 alumina disk separated each end guard heater from the specimen stack. The end guard heaters were backed by two $2\frac{1}{2}$-in.-thick $3\frac{1}{2}$-in.-OD alumina pieces, as shown in Fig. 1. The inside piece was cut from a dense 99% alumina brick, and the second, from a bubbled alumina brick. The end guard heaters, alumina disks, and backup pieces were suitably drilled to accommodate the core heater and its lead wires.

Apparatus Assembly

In assembling the apparatus, the specimen stack together with associated end pieces was built around a $\frac{5}{8}$-in. alignment rod to ensure axial symmetry between all components. As the stacking proceeded, the various measuring planes were instrumented with thermocouples as described below. After the top guard heater and backup pieces were in place, the alignment rod was removed and replaced by the core heater which was aligned axially by close-fitting alumina bushings contained in the top and bottom dense brick. Figure 2(*a*) shows the Armco iron specimen with the alignment rod still in place. When the stack assembly was completed, the muffle furnace sections were lowered over it, and granular alumina was poured into the annulus between the specimen and the muffle and between the specimen and the core heater. The water-cooled chamber was lowered into position, power and voltage connections were made, and the chamber was filled with bubbled alumina.

Thermocouple System

Several of the specimen disks were instrumented with thermocouples which were fitted into 0.063-in.-diam holes drilled in the disks perpendicular to the radial direction. The thermocouple wires extended out of the specimen stack through shallow grooves in the measuring planes. Figure 3 shows the thermocouple groove and hole arrangement for the measuring planes of the iron and UO_2 specimens. For UO_2 there were three measuring disks, each containing four $\frac{3}{8}$-in.-deep thermocouple wells – two at an inside radius of 0.450 in. and two at an outside radius of 1.375 in. These measuring disks were placed in the central 3 in. of the stack with two noninstrumented disks between each pair of measuring planes. For the iron there were two 1-in.-thick measuring

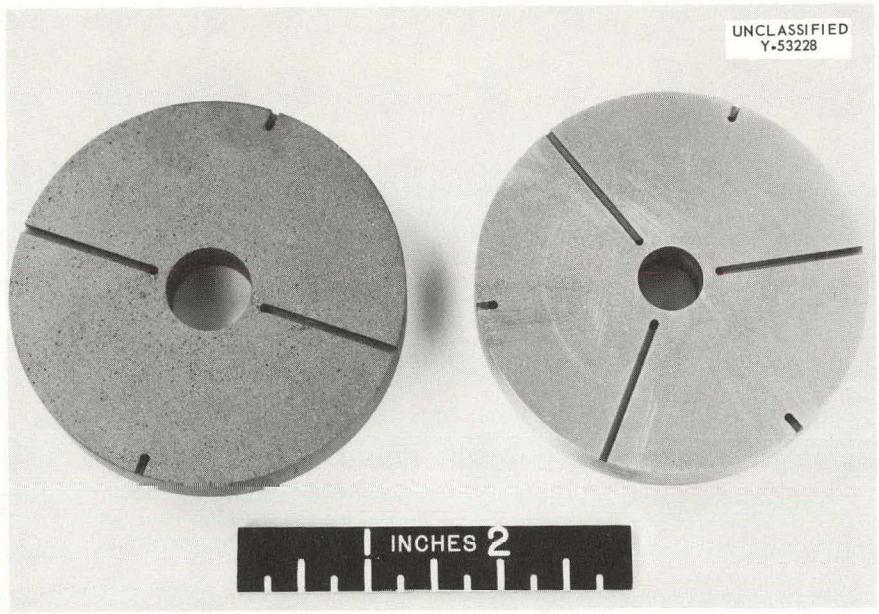

Fig. 3. Armco Iron and UO_2 Measuring Plane Disks, Showing the Thermocouple Groove and Hole Arrangements for the Radial Heat Flow Apparatus.

disks, each containing six $\frac{3}{4}$-in.-deep thermocouple wells – three on an inside radius of 0.500 in. and three on an outside radius of 1.313 in. These disks were also placed in the center 3 in. of the stack and were separated from each other by a noninstrumented, 1-in.-thick disk, as shown in Fig. 2(*a*).

Precise temperature measurement is the most critical aspect of the experiment. The thermocouples used were made from Sigmund Cohn reference-grade annealed Pt and Pt–10% Rh wire except for some low-temperature experiments on UO_2 where copper/Constantan thermocouples were used because of their greater sensitivity and the fact that tabulated emf's exist. The hot junctions of the thermocouples were positioned near the bottom of the holes in the measuring disks. The wires from these junctions were insulated electrically by two one-hole 0.031-in.-OD × 0.015-in.-ID Degussit Al23 alumina tubes. The hot junction was insulated electrically from the specimen by a $\frac{1}{16}$-in.-long, one-hole, 0.062-in.-OD × 0.030-in.-ID alumina tube at the bottom of the hole which also served to position the junction along the axis of the hole.

The thermocouples were made from 0.010-in.-diam wire which was tweezer-welded to 0.020-in.-diam wire just outside the stack. The smaller wire was used to minimize conduction losses from the hot junction, and the larger wire was used to decrease the probability of developing compositional or structural inhomogeneities in the region where the wire passes through severe temperature gradients. The 0.020-in.-diam wires were insulated in two-hole Morganite ΔRR

alumina tubing which was placed in the annulus between the muffle and the specimen and extended below the Al_2O_3 insulating pieces. From below these pieces the thermocouple wires extended through woven quartz tubing to fired lavite (hydrous aluminum silicate) tie-down blocks on the water-cooled brass baseplate as shown in Figs. 2(*a*) and 2(*b*). At these blocks the wires were mechanically connected to Pt and Pt–10% Rh wires which extended to the cold junction terminal board. This mechanical connection was made by pressing one wire on top of the other under lavite pieces screwed to the tie-down blocks such that the wires were in contact with no second metal. Several thermocouples were later added to the system and employed a different type of tie-down block as may be seen at the rear of the baseplate in Figs. 2(*a*) and 2(*b*). This tie-down block was made from Micarta,* and the thermocouple wires were clamped under nylon-coated steel screws. When the apparatus was reinstrumented or a new specimen installed, it was necessary only to replace the thermocouple wires from the specimen to these tie-down blocks. The thermocouple wires passed through the baseplate in seals which are described in detail in Appendix A. Mechanical connections of these wires to the Pt and Pt–10% Rh wires of the cold well were made at a shielded Micarta terminal board under nylon-coated steel screws. The cold junction was made by twisting the thermocouple wires to 0.020-in.-diam vinyl-insulated copper wires. The cold junctions were insulated from each other by vinyl tubing and were placed two each in 7-mm glass tubes partially filled with mineral oil for thermal contact. The glass tubes were fitted in a drilled copper block which was immersed in an ice bath. This copper block served to ensure that all of the cold junctions were at the same temperature such that the greatest accuracy could be attained for the differential emf measurements. It also served as a thermal inertia block in maintaining the cold junction temperature constant during the time the ice bath was being changed. The copper wires from the cold junction extended to vermiculite-filled switch boxes housing eight L&N thermal-free two-pole twelve-position switches which allowed absolute and differential thermal emf measurements to be made. Connections at the switches were made using L&N thermal-free solder.

The copper wires were 24-gage solid conductors from Western Electric Corporation telephone cable which contained 25 pairs of color-coded wires. This cable was very convenient to use because of the large number of thermocouples involved. Tests showed that the copper wires in this cable were homogeneous and exhibited thermal emf's of <0.02 μv when coupled with L&N thermal-free solder, switch lugs, and potentiometer terminals.

A Rubicon six-dial potentiometer with a certified accuracy of $\pm 0.01\% + 0.01$ μv was used in conjunction with an L&N upright galvanometer and a 20-ft optical lever to obtain a 0.01-μv null balance on all thermocouple emf's.

To minimize the effects of stray emf's and electrostatic fields, all lead wires were sheathed with braided copper shielding, and all switch boxes and related components were tied to one earth

*Micarta is a trade name for phenol-formaldehyde compound laminated fabric base, thermosetting plastic, manufactured by Micarta Division of Westinghouse Electric and Manufacturing Company.

ground with large conductors. The potentiometer was used to assure that parasitic or residual emf's due to placement of the wires were minimized and were less than 0.01 μv.

Power and Temperature Control Systems

The power to the core heater was supplied by a magnetic and transistor regulated dc power supply (Electronics Research Associated model 36-12M) which has ±0.05% load and line regulation and ±0.005% rms ripple. In-line tests showed that the unit is very acceptable for this application. In the early stages of the development of the apparatus, a bank of 12-v storage batteries, tapped such that multiples of 2 v could be obtained, were used to supply power to the core heater. However, the voltage drift of these batteries was found to be excessive for this steady-state method.

The dc power to the central 3-in. section of the core heater was determined by measuring the voltage drop between the voltage taps and the voltage drop across a 0.01-ohm L&N standard resistor, model 4222, through which the core heater current passed. These voltages were read using a L&N type K-3 potentiometer.

The overall temperature of the specimen was automatically controlled by the independent adjustment of the power to the three sections of the muffle furnace (in early runs on UO_2 the muffle consisted of only one 10-in. section). A Pt vs Pt–10% Rh thermocouple was attached to each muffle heater section and was connected in series opposition with a Zener diode voltage source.* The output of the diode source was adjusted so that the differential emf was zero when the desired temperature was reached. This differential emf was amplified by a L&N Microvolt Amplifier and fed to a –5 –0 +5 mv span L&N Speedomax H-DAT controller. Each DAT pulsed power from a suitable Variac power supply to achieve temperature control. In order to gain fine control and to reduce the effects of pickup by the thermocouples, only a small fraction of the total power to the heaters was pulsed. This was accomplished by the use of adjustable shunt resistors in parallel with the control relays of the power supplies. By this method the temperature control was ±0.01°C (±0.1 μv) at the heater thermocouples; this resulted in ±0.002°C (±0.02 μv) control within the specimen stack which could be maintained constant for several hours. At high temperatures, to reduce pickup by the thermocouples, it was sometimes necessary to substitute a dc power supply to drive the muffles. This power supply was a full-wave silicon diode bridge rectifier capable of supplying 35 dc amps at 140 v and was installed at the output of the Variac power supplies.

Axial heat flow in the specimen was restricted by the end guard heaters, and two different thermocouple arrangements were used to achieve control of these heaters. In the first method 0.010-in.-diam Pt vs Pt–10% Rh differential thermocouples were placed in comparable positions in the top and center disks and the bottom and center disks in the specimen stack. Each

*ORNL I&C Division Stable Millivolt Reference Supply, model Q-2156-2.

differential thermocouple was connected to a L&N Microvolt Amplifier which fed a −5 −0 +5 mv span L&N Speedomax H-DAT controller which pulsed power from a Variac power supply to the guard heaters to maintain a zero differential emf. This method of control required minimum attention and performed well at temperatures below about 600°C, but at higher temperatures it became unsatisfactory due to electrical leakage through the alumina insulators which tended to short the differential junctions. In order to circumvent these difficulties, 0.020-in.-diam thermocouples with grounded junctions were inserted in holes drilled in the end guard heaters and were used for absolute temperature control above 600°C. These thermocouples were used in the Zener diode-type control systems as were described for the muffle heaters.

METHOD OF OPERATION AND DATA ANALYSIS

The thermal conductivity was calculated by using the following equation for steady-state radial heat flow in a continuous isotropic medium which is devoid of heat sources or sinks.

$$k = \frac{Q}{2\pi L^*} \frac{\ln r_2/r_1}{\Delta T}, \tag{1}$$

where Q/L^* is the radial heat flow per unit time per unit length in the specimen, and ΔT is the temperature difference between the two radial positions, r_1 and r_2. This equation was derived from Fourier's equation for radial flow in a right circular cylinder, which is

$$\frac{Q}{L^*} = -k2\pi r \frac{dT}{dr} = \text{constant}. \tag{2}$$

In calculating k, Q is assumed to be equal to the joule heat dissipated per unit time in the length L^* of the core heater between the voltage taps. The values of r_1 and r_2 were taken as the position of the centers of the inside and outside thermocouple holes with respect to the axis of the specimen. Since r_1 and r_2 appear only as a ratio, the measurements are independent of the thermal expansion of the specimen, which constitutes an advantage over longitudinal methods. However, the thermal expansion of the core heater will change L^*. This correction amounts to <1% at 1000°C and was included in the calculation of k, by making L^* of Eq. (2) temperature dependent using data supplied by the manufacturer for the thermal expansion of Coors AD-99 alumina. The ΔT in Eq. (1) was obtained by averaging the readings of the inner thermocouples, subtracting the average of the outside readings, and dividing the resulting difference by the thermocouple sensitivity or Seebeck coefficient. The thermocouple sensitivity was obtained in two ways. In the first method the sensitivity was obtained by graphically smoothing the first differences taken from the NBS Bulletin No. 561, Table 1 (ref 11). In the second method the sensitivity was obtained by taking

[11] H. Shenker *et al.*, "Reference Tables for Thermocouples," *Natl. Bur. Std. (U.S.), Circ. 561* (Apr. 27, 1955).

the first derivative of an equation by Flynn[12] which fits NBS Bulletin No. 561 (Table 1) between 0 and 1450°C to within about ±10 μv. The two sensitivities obtained agreed for all temperatures to 1150°C to within 1%.

The value of k calculated by Eq. (1) corresponds to a temperature which is the arithmetic average of the temperatures at r_1 and r_2, if k is no higher order than a linear function of temperature over the range ΔT. Thus, in the experiment the ΔT was kept very small so that the temperature dependence of k could be very accurately determined and at the same time minimize thermal stresses in the specimen. For Armco iron, the ΔT's were ¾ to 4°C and for UO_2, 2 to 6°C below 800°C and 6 to 20°C above 800°C. For such small ΔT's, calibration differences between the thermocouples were extremely important. For this reason the thermocouples were intercompared at so-called isothermal conditions before each data point was taken. Thus at a given temperature an isothermal test was performed by comparing the thermocouple readings with no power to the core heater. Then power was supplied to the core heater, and the average stack temperature was readjusted to the same value as for the isothermal test. The ΔT used in Eq. (1) was then obtained by the relation,

$$\Delta T = \Delta T_{data} - \Delta T_{iso} , \tag{3}$$

where ΔT_{data} is the difference of the averages of the inside and outside thermocouple readings, with the core heater on, divided by the sensitivity, and ΔT_{iso} is the corresponding difference with the core heater off. A set of sample calculations and data sheets are given in Appendix I.

The isothermal test also corrects for radial heat flow which might be present even when the core heater is turned off. For example, when the core heater was off, the specimen may not have been truly isothermal because of imperfect guarding and insulation; however, since Eq. (1) is linear in Q and $1/\Delta T$, the isothermal correction merely subtracts the effect of these extra heat flows. Furthermore, even though the "isothermal" heat flows are not entirely radial, the ΔT_{iso} will correct for their effect if the nonradial portion is not appreciably changed by turning on the core heater. Experimental evidence for this was obtained by purposely running the apparatus with varying guarding conditions. It was found that, if the isothermal test was made under the same guarding conditions used when the core heater was on, the resulting value of k was largely independent of guarding. Thus for a fixed Q applied to the core heater, ΔT was constant even though ΔT_{iso} and ΔT_{data} were severely changed by different guarding conditions. It should also be mentioned that at a given temperature the data fit Eq. (1) very well. That is, ΔT was directly proportional to Q, and the k obtained was independent of the magnitude of Q. Obviously, the isothermal corrections were much more important at low values of ΔT and Q.

ACCURACY AND REPRODUCIBILITY

The accuracy of the method cannot be stated with absolute certainty. The maximum possible error in k due to inaccuracies in the measurements of the quantities which are used in Eq. (1) can

[12] D. R. Flynn, private communication, Apr. 10, 1963.

be assessed, and this is done in Appendix B. This error is between ±3.8 to 4.9% with a most probable value of ±0.9 to 1.3%, assuming that the errors are random. The real difficulty is in assessing how closely the experimental conditions fulfill the boundary condition used to derive Eq. (1). An indirect way to ascertain the overall accuracy of the method is to compare the results for some standard material with those of other laboratories. It will be pointed out below that the values obtained for UO_2 and Armco iron in this work were acceptably close to those obtained by other authors. For Armco iron, which is considered by many to be a thermal conductivity standard, this agreement indicates that the above probable error estimate is also a reasonable absolute accuracy statement.

However, one would like to be able to check directly how closely the experiment comes to fulfilling the boundary conditions. This can be done by observing the effect on the results of systematic changes in the apparatus or its operation which cause the boundary conditions to be more nearly fulfilled. For example, a possible source of error in the experiment was deviation from radial heat flow caused by improper guarding. For this reason the length of the muffle heater was doubled, and the length of the core heater increased from 10 to 15 in. between runs 4 and 5 on UO_2. The data given in Tables D.4 and D.5 Appendix D show that that this changed the results by <0.6%. Furthermore, it was shown that the results were largely insensitive to the longitudinal temperature profile in the stack so long as both the data and isothermal tests were taken under the same guarding conditions.

Auxiliary experiments described in Appendix C were performed to assess the possible error due to the $\frac{3}{8}$-in. thermocouple immersion depth in the UO_2 specimen. It was found that the error was on the order of 0.1%. In view of these test results the most probable accuracy of the technique appears to be that associated with the determinate errors, ±0.9 to ±1.3%.

If reproducibility or repeatability is defined as the percent change in the results for several sets of measurements without any intentional change in the system or operating conditions, then the reproducibility of this system was better than ±0.1%. These repeat measurements were made under approximately steady-state conditions (i.e., drift rates <0.1°C/hr), and several hours were allowed to elapse between measurements. The 0.1% is of the same order as the estimated uncertainties in determining the power and thermocouple emf's, as can be seen from rows 1, 6, and 7 of Table B.1, Appendix B. This excellent repeatability is one of the best features of this radial heat flow apparatus.

EXPERIMENTAL RESULTS ON UO_2

Specimen Characterization

The UO_2 disks were made by cold pressing nuclear grade depleted UO_2 powder and by sintering in hydrogen at 1850°C for 4 hr. This resulted in a solid with open and closed pores which

was 93.4% of the theoretical density (10.97 g/cm^3). The powder was produced by the thermal decomposition and reduction of ammonium diuranate (ADU). Table 1 gives the analyzed impurity contents of the original specimen. The O/U ratio was determined to be 2.01 ± 0.01. The ±0.01 indicates the range by which several different analyses of O/U differed. However, the reproducibility of any given method was much better than this. Reliable measurements of the change in O/U of the specimen which occurred during run 1 as discussed below were obtained by a thermogravimetric analysis technique before and after run 1. Figure 4 shows a photomicrograph of this UO_2 and indicates a mean grain diameter of 10 to 20 μ.

Table 1. Chemical Analysis of UO_2 Specimen

Impurity	(ppm)	(Atoms per Molecule of UO_2)
		$\times 10^{-5}$
Mo	5.6	1.8
Cr	2–14	4.2
Ni	2–11	3.7
Al	6	6.0
Cu	300	203
Na	1	1
C	40	90
N	30	58
F	<20	<28
Fe	265	128
Si	<10	<13
Ag	<0.5	Negligible
B	<0.5	Negligible
Cd	<10	<2.4
Nb	62	18
Cu	0.2	Negligible
Eu	<0.5	Negligible
Gd	<0.3	Negligible
Pb	<5	<0.7
Sm	<4	<0.7
Sn	37	8.4
	Total	565.9
O (excess)	593	1000

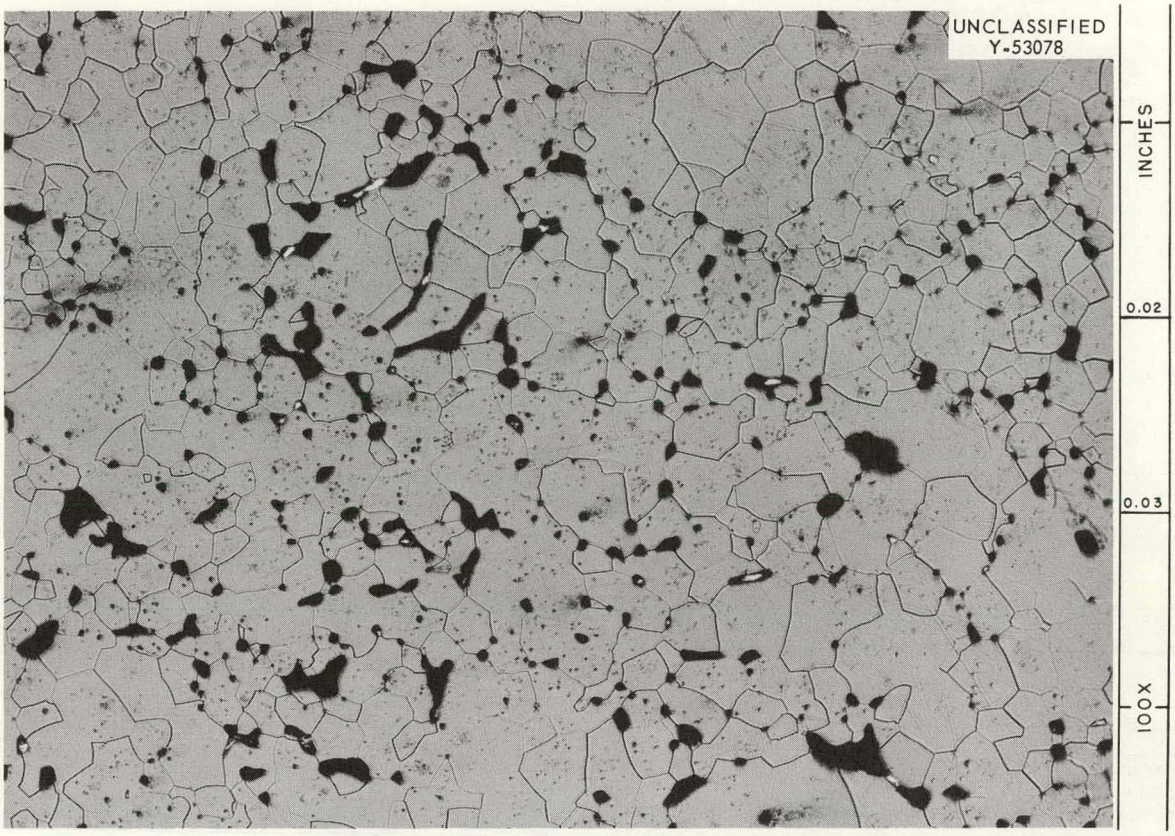

Fig. 4. Photomicrograph of the UO_2 Specimen.

Thermal Conductivity Data

All of the data reported here was corrected to theoretical density by dividing the actual experimental values by 0.934, the fraction of theoretical density. Ross[13] has shown that this type of correction may be considerably in error, especially for specimens having average grain sizes less than 15 μ. However, his measurements were made at 60°C, and the effects of grain size might be expected to decrease significantly at higher temperatures as the phonon mean free path becomes shorter.

It was found that between 200 and 1000°C a plot of thermal resistance, $1/k$, vs absolute temperature T for any given run gave a straight line to within 1% so that in this range

$$\frac{1}{k} = R - A + BT \, . \tag{4}$$

Seven separate runs on the specimen were made, and the system usually underwent some slight modification between runs either by reinstrumenting with new thermocouples and/or by changes

[13] A. M. Ross, *The Dependence of the Thermal Conductivity of Uranium Dioxide on Density, Microstructure, Stoichiometry and Thermal Neutron Irradiation*, CRFD-817 (AECL-1046) (September 1960).

Table 2. Values of A and B of Eq. (4) for Various UO_2 Runs Compared to Other Studies

Author	Run	$A\left(\frac{^{\circ}K\ cm}{w}\right)$	B (cm/w)
ORNL	1[a]	5.46	0.0223
ORNL	2	4.42	0.0225
ORNL	3	5.14	0.0225
ORNL	4	4.53	0.0237
ORNL	5	5.69	0.0221
ORNL	6	5.11	0.0221
Howard and Gulvin[14]		8.96–3.03	0.0196–0.0213
Kingery[15]		2.36	0.0222
Hedge and Fieldhouse[16]		7.98	0.0239
Deem and Lucks[17]		4.78	0.0246

[a]Run 1 between 200 and 400°C upon first heating.

to other components of the apparatus. Run 7 was a low-temperature run using copper/Constantan thermocouples on one measuring plane. All other runs were above room temperature, and Pt vs Pt–10% Rh thermocouples were used. The actual data for all the runs are given in Appendix D. For these six high-temperature runs, values of A and B in Eq. (4) are given in Table 2. The value of the intercept A varies considerably; whereas, with the exception of run 4, the value of the slope B was 0.0223 ± 0.0002 cm/w. For run 4, B was 0.0237 and was based on only three measurements; however, considering the excellent agreement between the other runs, this value is discounted.

Howard and Gulvin[14] give values of A and B for their work and for other authors, and these are also shown in Table 2. Here again the agreement for values of B is much better than agreement on values of A.

Run 1 gave a linear resistance plot between about 200 and 400°C with a slope of 0.0223 cm/w, in agreement with the other values; however, as the specimen was heated above 400°C, the resistance showed a negative deviation from this line as shown in Fig. 5. Above 600°C the resistance was again linear with essentially the same slope as below 400°C. Therefore the new line was shifted downward but remained parallel to the 200 to 400°C line. Upon cooling and during reheating of the specimen in run 2, the data followed this second line. The shift

[14]V. C. Howard and T. F. Gulvin, *Thermal Conductivity Determination on UO_2 by a Radial Heat Flow Method*, IG-51(RB/C) UKAEA Culcheth (Feb. 10, 1961).

[15]W. D. Kingery *et al.*, "Thermal Conductivity: X, Data for Several Pure Oxide Materials Corrected to Zero Porosity," *J. Am. Ceram. Soc.* 37, 107 (1954).

[16]J. Hedge and I. Fieldhouse, *Measurement of Thermal Conductivity of Uranium Dioxide*, AECU-3381 (Sept. 20, 1956).

[17]H. W. Deem and C. F. Lucks, *Thermal Conductivity of Uranium and UO_2*, BMI-1324 (Mar. 1, 1959).

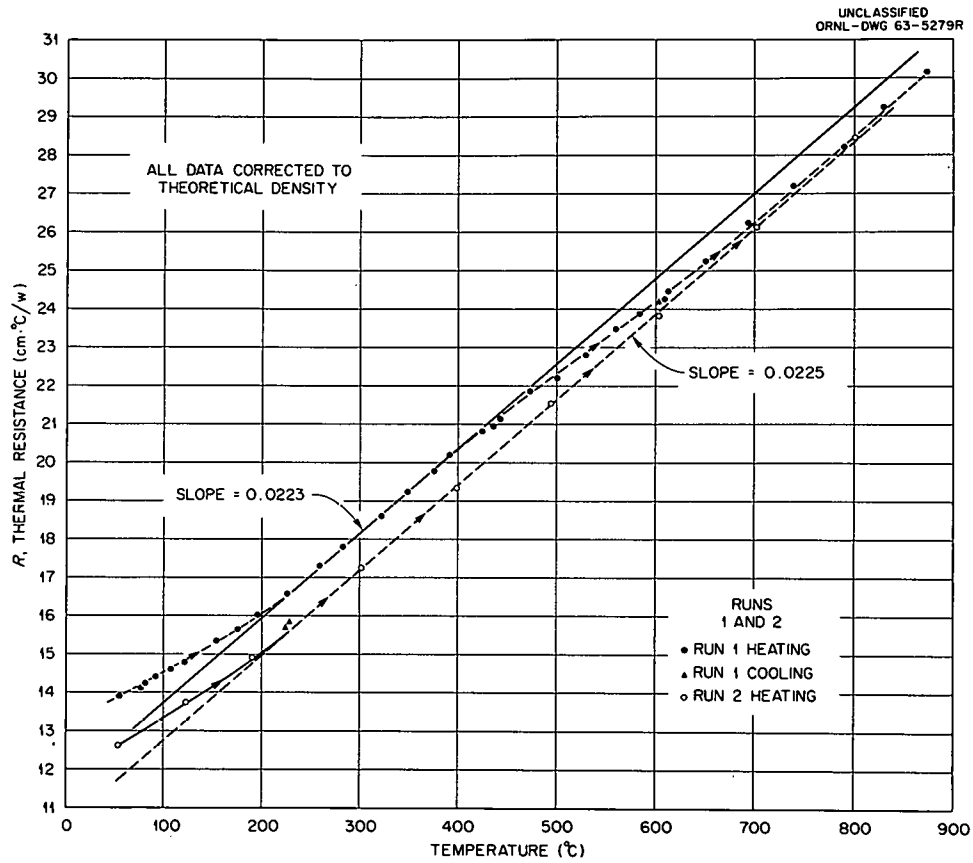

Fig. 5. Thermal Resistance of UO_2 as a Function of Temperature for Runs 1 and 2 in the Radial Heat Flow Apparatus.

is believed to have been due to a decrease in the excess oxygen content of the specimen produced during heating in run 1 because of the scavenging effect of a tantalum liner between the specimen and the muffle heater. Upon cooling to room temperature after run 1, the tantalum liner was found to have been severely oxidized. A small portion of one of the specimen disks was analyzed for the O/U ratio, and this was found to be 2.006 compared to 2.012 for the specimen prior to run 1. The initial UO_2 specimen (before first heat) yielded O/U ratios of 2.012 ± 0.002 (wt gain on ignition in air) and 2.002 ± 0.002 (chemical analysis). After the first heat the O/U ratios were 2.006 ± 0.002 (wt gain on ignition in air) and $<2.001 \pm 0.002$ (chemical analysis). The values determined by the ignition-in-air method are believed to indicate the change in the O/U ratio more precisely than the chemical analysis method. The uncertainty stated above in the original composition, ±0.01, was the average spread of the two analytical methods.

Figure 5 shows that the data for runs 1 and 2 below 200°C deviate in a regular way from the straight line. Béthoux, Thomas, and Weil[8] recently found a maximum in the thermal conductivity curve of UO_2 at about room temperature. Such a maximum would plot as a minimum in the thermal resistance plot, and this is indicated by the 55 to 200°C data of runs 1 and 2. To check this point,

in run 7 one plane was reinstrumented with copper/Constantan thermocouples, and the annular space between the muffle and the brass chamber wall was filled with dry ice. This permitted data to be obtained to -57°C; the results of runs 6 and 7 are shown in Fig. 6. These data show a minimum near 320°K although more scatter was observed at these temperatures.

In runs 3 to 5, the apparatus was heated to temperatures above 1000°C. In run 5, a temperature greater than 1400°C was probably reached; however, during this run, rapid thermocouple drift was observed at the higher temperatures. The apparatus was cycled between 900 and 1350°C several times in an attempt to stabilize the thermocouples with the results shown in Fig. 7. The net effect of the thermocouple drift was to cause a hysteresis-type behavior, with each heating cycle yielding lower $1/k$ values than the preceding one. Upon final cooling, the results followed a line parallel to, but about 6% lower than, that obtained on the first heating of run 5. To check the extent of the thermocouple drift which had occurred at high temperatures, the top two measuring planes were reinstrumented after run 5, and the bottom plane was left intact. New thermocouples were attached to the outside surface of the bottom measuring disk and to the outside surface of the top measuring plane. During run 6 the readings of these thermocouples were compared to those of the old thermocouples on the bottom plane under isothermal conditions. The outside thermocouples on the top disk read the same as those within the disk to within ± 1 μv, whereas for the bottom plane a difference was observed which measured the error of the old thermocouples. This error increased with temperature and, on the average, amounted to 370 μv (or 37°C) at 600°C. Figure 8 shows a plot of the error of the old thermocouples compared to NBS

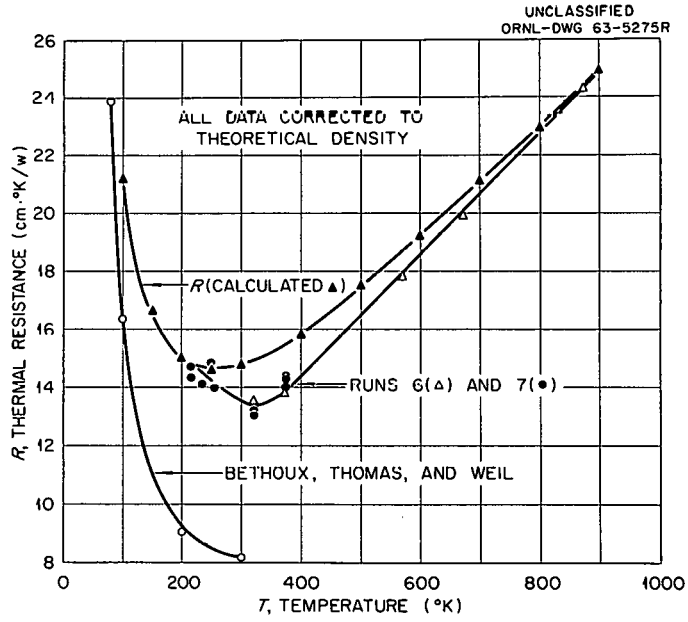

Fig. 6. Thermal Resistance of UO_2 as a Function of Temperature for Runs 6 and 7 in the Radial Heat Flow Apparatus and Calculated Thermal Resistance.

Bulletin No. 561, Table 1, values. This error enters the k data in two ways. First, the wrong sensitivity was used to compute ΔT in Eq. (1); and second, the absolute temperature at which k was measured was actually higher than it appeared. Because of these errors, the data taken in runs 3 to 5 above about 1100°C and in run 5 upon cooling from high temperature are not valid.

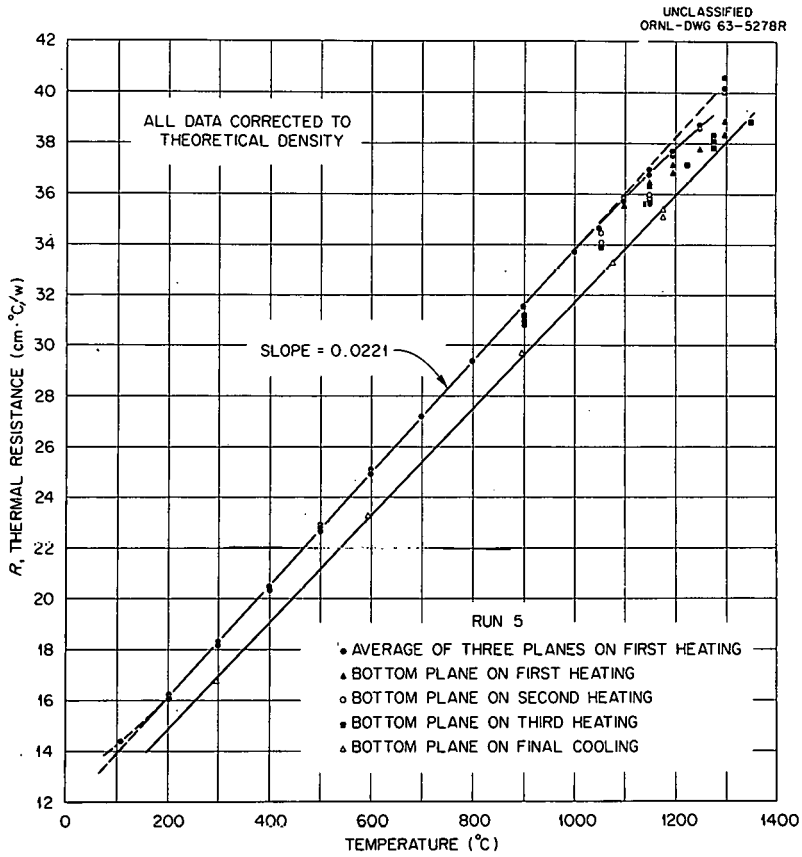

Fig. 7. Thermal Resistance of UO_2 as a Function of Temperature for Run 5 In the Radial Heat Flow Apparatus.

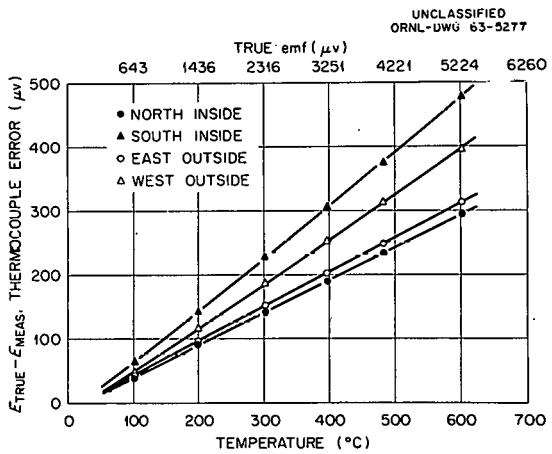

Fig. 8. Thermal EMF Error in the Run 5 Thermocouples Caused by a High-Temperature Exposure, as Determined During Run 6 in the Radial Heat Flow Apparatus.

Because the thermocouple emf's did not drift below 1100°C, the data taken in runs 3 to 5 below 1100°C are considered valid. The data between 1000 and 1100°C were 1 to 3% below the extrapolation of the 200 to 1000°C straight-line portion. Figure 9 is a k vs temperature plot which shows the relative position of the k values obtained in this work (shaded band) compared to other investigations. All values are corrected to theoretical density as discussed above.

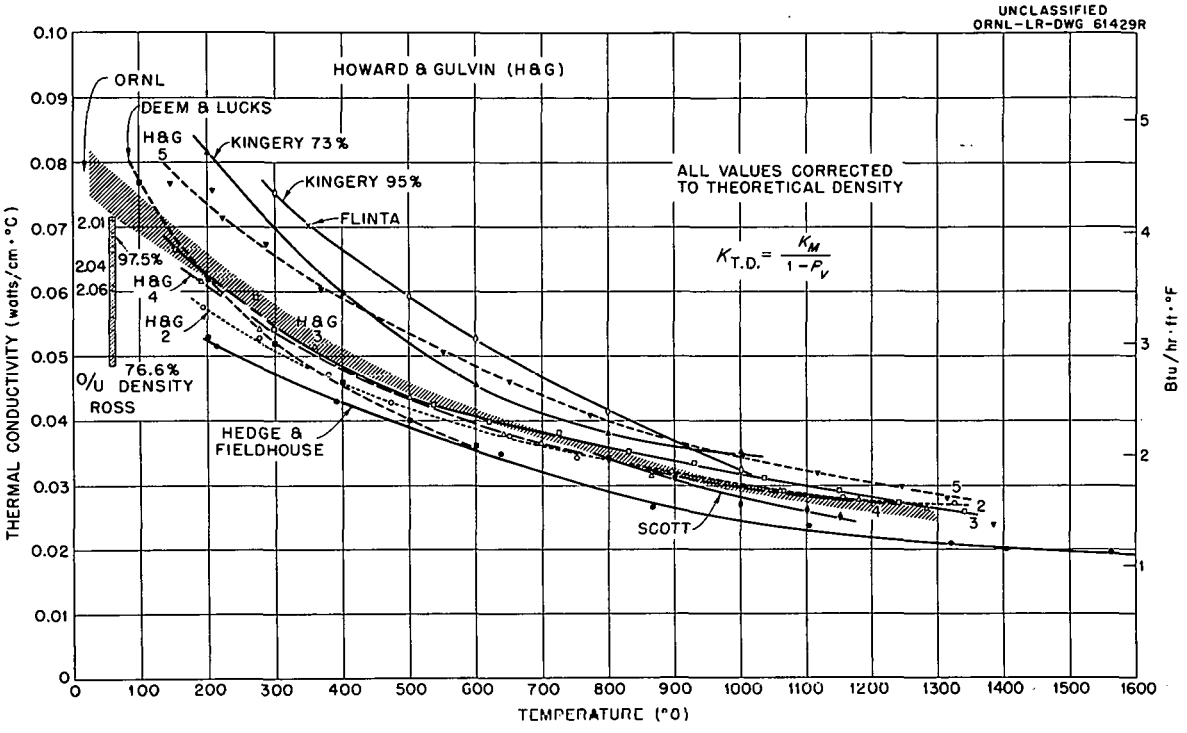

Fig. 9. Thermal Conductivity of UO_2 as a Function of Temperature as Reported by Various Authors. Note the effects of O/U ratio and density at 60°C. The data of Flinta was obtained from *Thermal Conductivity of UO_2*, TID-7546 (Book 2) (November 1957), pp 516–25; and that of Scott from *The Thermal Conductivity of UO_2*, AERE/M/R 2526 (March 1958). The data of Ross; Howard and Gulvin; Kingery; Hedge, and Fieldhouse; and Deem and Lucks were obtained from references 13–17, respectively.

To obtain higher temperature data, the present thermocouple error must be reduced, and this may be possible through the use of more stable thermocouples such as Pt–30% Rh vs Pt–6% Rh. It is also possible to incorporate into the system a temperature standard against which the thermocouples can be calibrated during isothermal conditions. Such a standard is the electrical resistance of the Pt–10% Rh core-heater wire. It was found that this is a sensitive, reproducible resistance thermometer. By use of this thermometer, it is possible to check the thermocouples *in situ* during a run and, if need be, recalibrate them when the system is isothermal. Therefore, if the thermocouple drift is not too rapid, data can be taken by preceding each data point with such an isothermal calibration.

The resistivity of the Pt–10% Rh wire was obtained from measurements of the core-heater resistance at isothermal conditions, and the data were fit by a least-mean-squares criterion to a second-order polynomial in temperature. This expression is

$$\rho = 18.50 + 3.100 \times 10^{-2}\, t - 3.520 \times 10^{-6}\, t^2 \,. \tag{5}$$

The fit was made using experimental data in the temperature range 111 to 800°C. Later, higher temperature values were measured, and these agreed with the extrapolation of the lower temperature equation to within ±0.2% to 1000°C. These data agree to within ±0.4% of that reported by Roeser and Wensel.[18] The experimental values are given in Appendix H.

DISCUSSION OF THE RESULTS ON UO_2

The data obtained in seven runs gave a consistent picture of the thermal conductivity of UO_2 from −57 to 1000°C. The results can be interpreted from the point of view that the only heat transport is by phonons.

It should be mentioned that none of the following calculations are rigorous, but they do show that the experimental results are in qualitative agreement with a simplified theory of thermal conductivity of electrically insulating solids.

For the Temperature Range 200 to 1000°C

Derivation of an Expression for Thermal Resistance

If two scattering mechanisms (i.e., interaction between the phonons themselves, umklapp processes, and interaction between phonons and impurities) are assumed, the average phonon mean free path $\bar{\ell}$, in terms of the average mean free paths for the two scattering processes $\bar{\ell}_u$ and $\bar{\ell}_I$, can be expressed by

$$\frac{1}{\bar{\ell}} = \frac{1}{\bar{\ell}_u} + \frac{1}{\bar{\ell}_I}, \tag{6}$$

if the additional assumption that the two processes are independent is made. Using an elementary but physically realistic model based on the thermal conductivity of a gas, the thermal conductivity of the solid can be expressed as

$$k = \frac{1}{3} c_V \bar{v} \bar{\ell} \,, \tag{7}$$

where c_V is the specific heat at constant volume per unit volume and $\bar{v}$ is the average velocity of phonons. Equation (7) also requires the assumption that the phonon scattering reaction at a

[18] W. F. Roeser and H. T. Wensel, "Table 15. Electrical Resistivity as a Function of Temperature," p 1312 in *Temperature – Its Measurement and Control in Science and Industry*, Reinhold, New York, 1941.

point in the solid restores local thermodynamic equilibrium to the phonon distribution corresponding to the conditions at that point.[19] If the further assumption is made that the scattering by impurities is independent of the phonon frequency (i.e., that the scattering cross section is independent of the phonon frequency), then $\bar{\ell}_I$ is independent of temperature provided that the impurity concentration does not change with temperature. Combining Eqs. (6) and (7), the thermal resistance becomes

$$R = \frac{3}{c_V \bar{v}} \left(\frac{1}{\bar{\ell}_u} + \frac{1}{\bar{\ell}_I} \right) = R_u + R_I , \tag{8}$$

where R_u is the umklapp contribution, and R_I is the impurity contribution which is independent of temperature. For an electrically insulating solid well above its Debye temperature, the following expression for three phonon umklapp processes has been derived by Leibfried and Schlömann:[20]

$$\frac{1}{k_u} = R_u = \frac{\gamma^2 T}{\frac{24}{10}(4)^{1/3}\left(\frac{k}{h}\right)^3 M \delta \theta_D^3} , \tag{9}$$

where

γ is the Gruneisen constant,

k is Boltzmann's constant,

h is Planck's constant,

M is the mass per atom,

δ^3 is the volume per atom,

θ_D is the Debye temperature.

For compounds, to a first approximation, M is the average mass per atom, and δ^3 is the average volume per atom. At high temperatures c_V and $\bar{v}$ are approximately constant so the thermal resistance can be expressed by

$$R = A + BT , \tag{10}$$

where A corresponds to the impurity resistance R_I, and BT corresponds to the lattice resistance R_u. This is exactly the form of R measured experimentally in runs 2 to 6 on UO_2 between 200 and 1000°C.

---

[19] J. R. Drable and H. J. Goldsmid, *Thermal Conduction in Semiconductors*, p 138, Pergamon Press, Oxford, 1961.

[20] G. Leibfried and E. Schlömann, "Wärmeleitung in elektrisch isolierenden Kristallen," (Heat Conduction in Electrically Insulating Crystals), *Akad. Wiss. Gottingen, Math.-Physik. Kl.* IIA, 71 (1954). (Translated for ORNL by the Technical Library Research Service under Purchase Order No. 34B-60150, Letter Release No. S-70.)

Calculation of Debye Characteristic Temperature

A Debye temperature of 216°K was calculated using Eq. (9). This value compares to 160°K from specific heat measurements[21] and to 188°K from x-ray results.[22] This calculation used the measured value of B, 14.94×10^{-23} g/atom for M, 1.37×10^{-23} cm^3/atom for δ^3, and 1.64 for γ. The value for γ was calculated using the equation,

$$\gamma = \frac{\alpha_v}{\kappa c_v}, \tag{11}$$

where α_v is the volume thermal expansion coefficient, and κ is the isothermal compressibility. A value for α_v of three times the linear expansion coefficient α_L was used, and α_L was taken to be 10.5×10^{-6}/°C, the average value for the range 25 to 1000°C.[23] The compressibility was taken as 0.62×10^{-5} cm^3/wsec (ref 24) and a value of 3.29 wsec cm^{-3} (°C)$^{-1}$ was used for c_v. This value of c_v was obtained by dividing C_v, the molar heat capacity at constant volume at 700°C, by V, the molar volume. Values of C_v were calculated from C_p data[21,25] using the relation

$$C_v = C_p - \frac{V\alpha_v^2}{\kappa} T, \tag{12}$$

where V was taken as the molar volume at room temperature, 24.8 cm^3/mole, and are plotted in Fig. 10.

Impurity Scattering Cross-Section Estimation

The average mean free path for n different types of scattering impurities may be written as

$$\frac{1}{\bar{\ell}_I} = \sum_i^n \frac{1}{\bar{\ell}_i} = \sum_i^n \bar{\sigma}_i N_i, \tag{13}$$

where $\bar{\sigma}_i$ is the average scattering cross section, and N_i is the impurity concentration for impurity type "i." To get an order of magnitude estimate for the $\bar{\sigma}$'s, they are all assumed to be the same. The concentration of impurities in the UO_2 specimen was estimated from analysis to be about 15

---

[21] W. M. Jones, J. Gordon, and E. A. Long, "The Heat Capacities of Uranium, Uranium Trioxide, and Uranium Dioxide from 15°K to 300°K," *J. Chem. Phys.* 20(4), 695 (1952).

[22] C. J. Sparks and B. S. Borie, "An X-Ray Determination of the Debye-Waller Factors for Cu_2O and UO_2 and the Atomic Scattering Factor for Cu in Cu_2O," pp 177–84 in *Advances in X-Ray Analysis* (ed. by William M. Mueller and Marie Fay), vol 6, Plenum Press, New York, 1963.

[23] J. Belle (ed.), *Uranium Dioxide Properties and Nuclear Applications*, p 176, GPO, Washington, D.C., July 1961.

[24] J. Belle, *ibid.*, p 208.

[25] G. E. Moore and K. K. Kelley, "High-Temperature Heat Contents of Uranium, Uranium Dioxide and Uranium Trioxide," *J. Am. Chem. Soc.* 69, 2105 (1947).

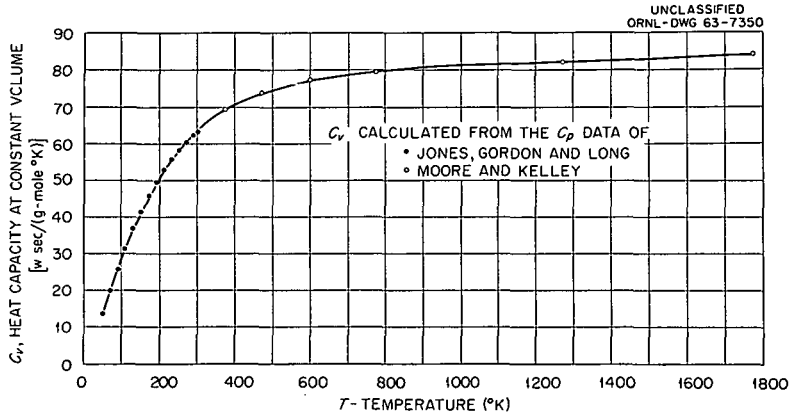

Fig. 10. Heat Capacity at Constant Volume per Gram-Mole of UO_2 as a Function of Temperature.

impurity atoms (including excess oxygen) per 1000 UO_2 molecules, which corresponds to 3.64×10^{20} impurities/cm^3. Using 81.6 wsec mole^{-1} (°K)$^{-1}$ for C_v, 4×10^5 cm/sec for $\bar{v}$, and 5 cm (°K) w^{-1} for R_I in Eq. (8), $1/\bar{\ell}_I$ was found to be 2.19×10^6 cm^{-1}. The value used for R_I is the average experimental value of the intercept A in our runs. The value of $\bar{v}$ was calculated as

$$\bar{v} = \left(\frac{E}{\rho^*}\right)^{1/2} \tag{14}$$

where E is the modulus of elasticity which was taken to be 25×10^6 psi (ref 26), and ρ^* is the UO_2 density. From Eq. (13) $\bar{\sigma}_i$ was calculated as

$$\bar{\sigma}_i = \frac{2.19 \times 10^6}{3.64 \times 10^{20}} = 6.02 \times 10^{-15} \text{ cm}^2/\text{impurity}.$$

This value seems reasonable since it is of the order of the square of the unit cell dimension for UO_2.

Effect of O/U Ratio on k

Since the experimental values of the intercept A varied from 5.67 to 4.42 cm °K w^{-1} for all runs, the following analysis was made to determine if changes in O/U ratio could cause these changes in A. Between runs 1 and 2 the O/U ratio changed from 2.012 to 2.006, corresponding to a ΔN of 6 excess oxygen atoms per 1000 UO_2 molecules. The change in resistance due to this ΔN is then calculated from Eq. (8) to be

$$\Delta R_I = \frac{3}{c_v \bar{v}} \Delta \left(\frac{1}{\bar{\ell}_I}\right) = \frac{3}{c_v \bar{v}} \bar{\sigma}_i \Delta N . \tag{15}$$

---

[26] J. Belle, *op. cit.*, p 206.

But we can express the average value of R_I as

$$\overline{R}_I = \overline{A} = \frac{3}{c_V \overline{v}} \overline{\sigma}_i N ,$$

so

$$\frac{3}{c_V \overline{v}} \overline{\sigma}_i = \frac{\overline{R}_I}{N} = \frac{\overline{A}}{N} .$$

Thus

$$\Delta R_I = \overline{A} \frac{\Delta N}{N} = 5 \times \left(\frac{-6}{15} \right) = -2 \text{ cm } ^\circ\text{K w}^{-1} .$$

The observed change was −1 cm °K/w, so this very rough calculation adequately describes both the direction and the order of magnitude of the change.

Several authors have observed a decrease in the thermal conductivity of UO_2 with increasing O/U ratio.[13,14,27,28] In particular the results of Ross[13] at 60°C show that a change in O/U ratio from 2.00 to 2.02 changed the thermal conductivity by about 6%, whereas Howard and Gulvin[14] indicate a 16% decrease. The observed shift between runs 1 and 2 at this temperature was about 10% for an O/U ratio change from 2.012 to 2.006.

Low-temperature measurements by Béthoux, Thomas, and Weil[8] on UO_2 have shown that, beside ordinary lattice and impurity scattering, there is also a scattering of phonons by the magnetic moment of the U^{4+} ions. Further, these authors suggest that the mean free path associated with this mechanism may be independent of temperature, as has been assumed here for impurity scattering. In this case, the intercept A should really be $R_I + R_m$, where R_m is the magnetic moment contribution. This means that the above calculations for $1/\overline{\ell}_I$ and ΔR are somewhat too large, which again agrees with experiment.

In the above calculation if the specimen is assumed to be pure and free of imperfections, the value of A is zero. However, many insulating solids yield negative A values and, furthermore, the linear dependence of R extends to temperatures considerably below the Debye temperature [e.g., Si (ref 29) and BeO (ref 30)]. For temperatures below the Debye temperature an equation of the form[31] is expected,

$$k_u = a \left(\frac{T}{\theta_D} \right)^n \exp \left(\frac{\theta_D}{bT} \right) , \qquad (16)$$

---

[27] J. Belle, "Properties of Uranium Dioxide," *Proc. Intern. Conf. Peaceful Uses At. Energy, 2nd Geneva, 1958* 6, 569 (1958).

[28] R. W. Nichols, "Ceramic Fuels – Properties and Technology," *Nucl. Eng. (London)* 3(8), 327–33 (1958).

[29] A. D. Stuckes, "The Thermal Conductivity of Germanium, Silicon and Indium Arsenide from 40 to 425°C," *Phil. Mag.* 5, 84 (1960).

[30] R. E. Taylor, "Thermal Conductivity and Expansion of Beryllia at High Temperatures," *J. Am. Ceram. Soc.* 45(2), 74 (1962).

[31] J. M. Ziman, *Electrons and Phonons, The Theory of Transport Phenomena in Solids*, p 291, Oxford at the Clarendon Press, 1960.

where a, n, and b are empirical constants not clearly defined by theory. Above the Debye temperature the Leibfried and Schlömann formula 9 should hold; this may be expressed as

$$k_u = k_0 \frac{\theta_D}{T}, \tag{17}$$

where k_0 is the thermal conductivity at the Debye temperature. Expressing the resistance as the reciprocal of k_u, the two equations will merge only if we make $n = -1$ and $a = k_0$. This can be seen by expanding the exponential in Eq. (16) using these values of the constants n and a.

$$\begin{aligned} R_u = \frac{1}{k_u} &= \frac{1}{k_0}\frac{T}{\theta_D}\left[1 - \frac{\theta_D}{bT} + \frac{1}{2}\left(\frac{\theta_D}{bT}\right)^2 - \dots\right] \\ &\approx \frac{1}{k_0}\frac{T}{\theta_D} - \frac{1}{k_0 b} \end{aligned} \tag{18}$$

for reasonably high values of T and b. If b is fairly large, R_u will be approximately linear well below the Debye temperature, and the intercept will be negative. At sufficiently high temperatures the constant term is negligible compared to the first term, which is the reciprocal of Eq. (17). A maximum value of b is 2 (ref 31) and yields a negative intercept of $-0.0223/2 \times 216 = -2.4$ cm °K w^{-1}, where 216 is θ_D and $\theta_D B$ is equal to $1/k_0$ by equating the slope of Eq. (18) with B. Therefore the impurity portion of the thermal resistance should be A, recorded in Table 2, plus the absolute value of this negative intercept. This would change the calculated values of $1/\bar{\ell}_I$ to 3.25×10^6 and σ_i to 8.92×10^{-15} cm^2/impurity. The value of ΔR_I would increase to 2.8 cm °K w^{-1}.

For the Temperature Range −57 to 200°C

The observed thermal resistance of UO_2 below 200°C may be adequately ascribed to the fact that C_v of UO_2 begins to drop rapidly below this temperature, as can be seen in Fig. 10. Using the value of $1/\bar{\ell}_I$ of 2.19×10^6 cm^{-1} derived initially and the values of $1/\bar{\ell}_u$ given by the relation,

$$\frac{1}{\bar{\ell}_u} = 9.67 \times 10^3 T \text{ cm}^{-1}, \tag{19}$$

the thermal resistance at low temperatures can be calculated using experimental values of C_v from Fig. 10. Equation (19) was derived by setting R_u of Eq. (8) equal to BT, where B was the high-temperature slope of the resistance plot, and using 3.29 wsec cm^{-3} °K^{-1} for c_v and 4×10^5 cm/sec for $\bar{v}$. The thermal resistance calculated in this way indeed shows an upswing at temperatures below about 300°K and of the same order of magnitude as was observed experimentally. Both theoretical and measured curves are shown in Fig. 7 together with the curve of Béthoux, Thomas, and Weil.[8]

For the Temperature Range 1000 to 1100°C

The thermal resistance at 1100°C for runs 3 to 5 all lie 1 to 3% below the extrapolation of the linear portion of the thermal resistance plot. It is thought that the thermocouples were still giving reliable results in these runs at 1100°C; therefore the deviation is real and probably due to an irreversible change in the specimen at these high temperatures. This supposition is based on the fact that run 6 made immediately after run 5 gave a resistance plot which was parallel to that of run 5 but which was lower by 0.6 cm °K w^{-1}. Evidently the high-temperature heat treatment of the specimen in run 5 produced this change, and on the basis of the above discussion this was a change in the impurity concentration.

The deviation of R from a straight line between 1000 and 1100°C could also be due to an electronic contribution to the thermal conductivity. The electronic contribution for a nondegenerate semiconductor may be written as[32]

$$k_e = \frac{2k^2}{e^2}\sigma T + \frac{k^2}{e^2}\frac{\sigma_h \sigma_e}{\sigma}\left(4 + \frac{E_G}{kT}\right)^2 T , \tag{20}$$

where σ is the electrical conductivity, and

$$\sigma = \sigma_e + \sigma_h , \tag{21}$$

where σ_e and σ_h are the portions of the electrical conductivity due to electrons and holes respectively. The term E_G is the forbidden band gap which for UO_2 is ~1.9 ev (ref 33). In Eq. (20), k_e will be a maximum if $\sigma_e = \sigma_h$. At 1000°C, assuming $\sigma_h = \sigma_e$ and a fairly high value of 1 $(ohm\text{-}cm)^{-1}$ for σ (ref 33), one obtains 0.0011 w cm^{-1} $°K^{-1}$ for k_e, which is about 3.8% of the observed value. The following tabulation shows values of k_e calculated using Eq. (20) and the assumption that σ has an activation energy of 0.95 ev.

t (°C)	k_e (w cm^{-1} $°K^{-1}$)	Percent of k
900	0.55×10^{-3}	1.7
1000	1.1×10^{-3}	3.8
1100	2.0×10^{-3}	7.2

Hence the 1 to 3% negative deviation of R from a straight line between 1000 and 1100°C could be explained as the influence of an electronic contribution.

---

[32] J. R. Drable and H. J. Goldsmid, *op. cit.*, p 118.

[33] R. A. Wolfe, *The Electrical Conductivity and Thermoelectric Power of Uranium Dioxide*, WAPD-270 (April 1963).

Finally, of direct interest to the above are two thermal conductivity studies on single-crystal UO_2.[34,35] Both show the thermal conductivity of the single crystal to be much higher than the polycrystalline material, even at moderately low temperature, and both show an increase at high temperatures. This very interesting difference needs to be explained quantitatively on the basis of the controlling heat transfer mechanism.

EXPERIMENTAL RESULTS ON IRON

Thermal conductivity measurements were made on Armco iron between 100 and 1000°C in the radial heat flow apparatus, and the results were analyzed in terms of two mechanisms contributing to the total thermal conductivity. To aid in this analysis, electrical conductivity measurements were made in the same temperature region on a sample fabricated from the same iron stock. The effects of the well-known solid-state changes which occur in iron on the mechanisms of thermal conduction made it a particularly interesting material for study.

Specimen Characterization

The Armco iron specimen had the composition listed in Table 3. With the exception of O, N, H, C, P, and S, these numbers were the result of semiquantitative analyses and may vary from one-half to two times the values listed.

[34] J. L. Daniel, J. Matolich, Jr., and H. W. Deem, *Thermal Conductivity of UO_2*, HW-69945 (September 1962).

[35] J. A. Christensen, *Thermal Conductivity of UO_2*, HW-76301 (August 1963), pp 2.30–2.33.

Table 3. Chemical Analysis of Armco Iron Specimen

Element	Concentration (wt %)
Emission Spectroscopy	
Semiquantitative	
Al	<0.05
Cr	<0.05
Cu	0.1
Mn	0.05
Mo	<0.05
Ni	0.1
Si	<0.02
Ti	<0.01
V	<0.02
Quantitative Analysis	
C	0.013
P	0.006
S	0.023
H_2	<0.0001
O_2	0.086
N_2	0.0050

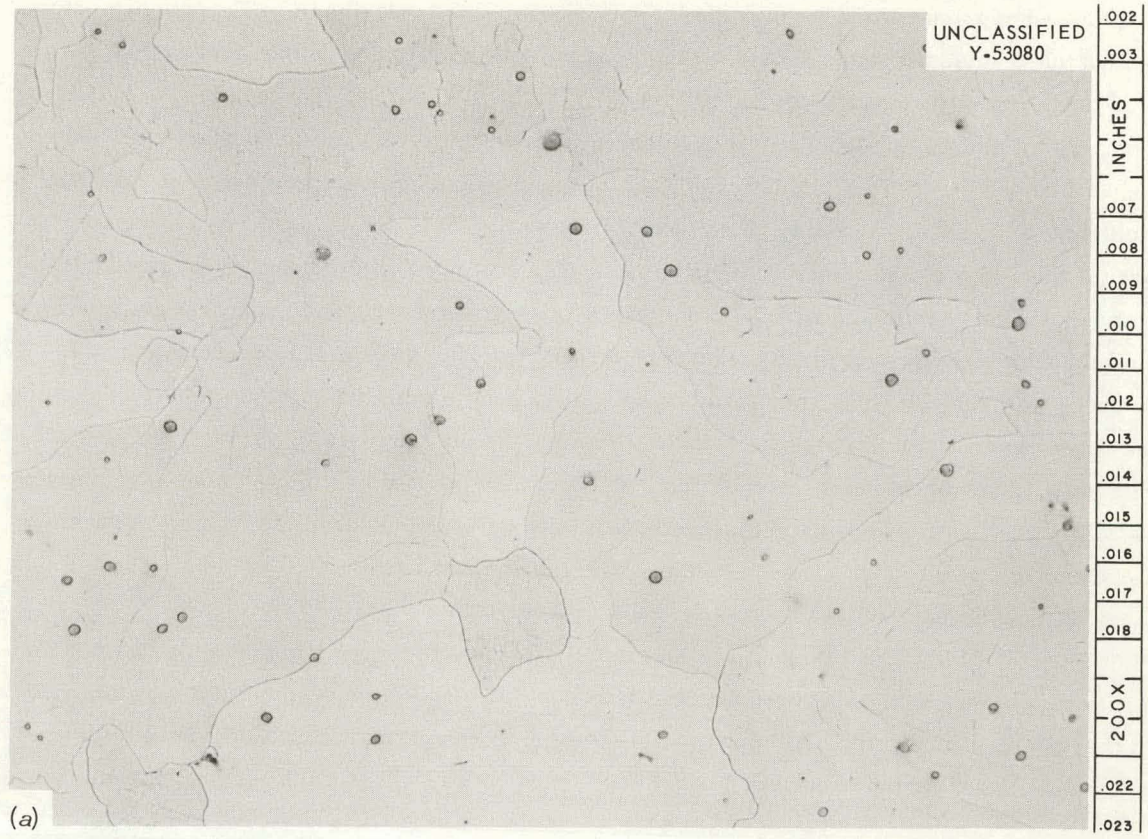

(a)

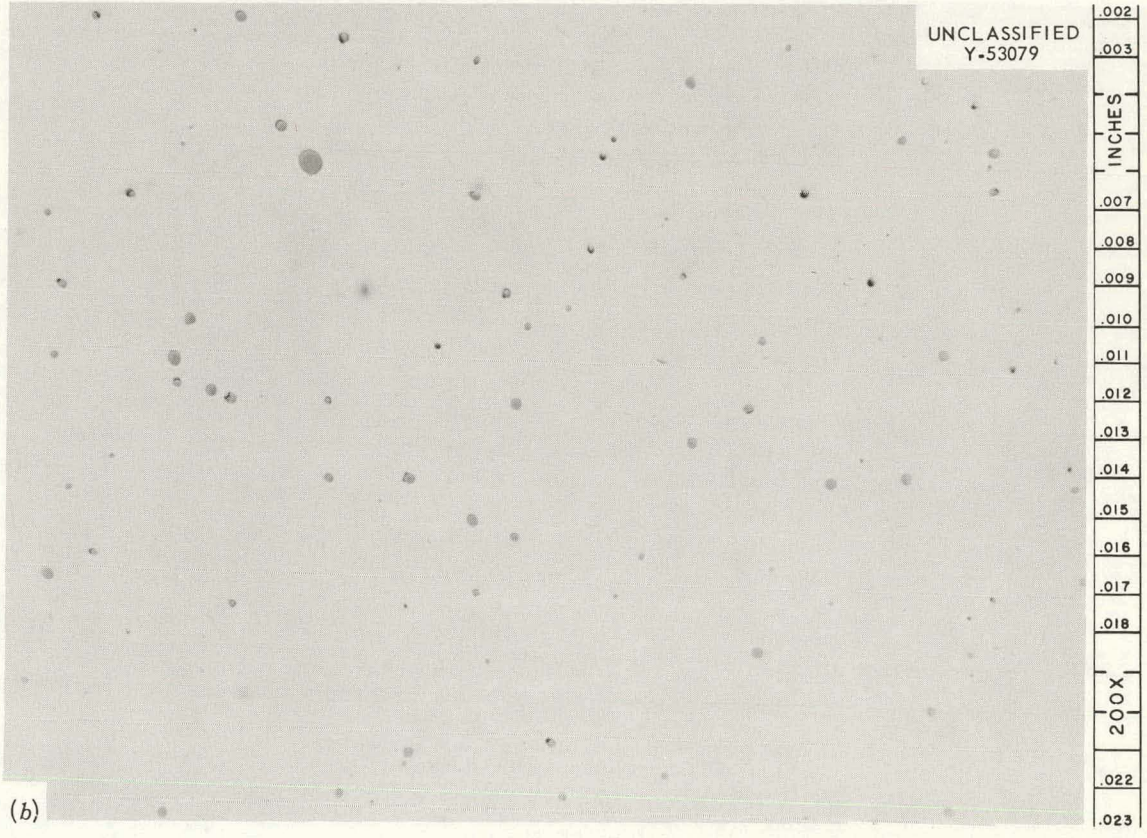

(b)

Fig. 11. Photomicrographs of Armco Iron. (*a*) Etched. (*b*) Unetched.

Photomicrographs of the iron specimen, as viewed at 200X, are shown in Fig. 11. The etched and unetched microstructures show that a second phase is present. A point-count method was used to determine the volume percent of this phase to be 0.90 ± 0.05. This phase was not uniformly distributed in the specimen, as evidenced by local variations in the volume percent which ranged from 0.86 to 0.97. Calculations based on the chemical analysis for oxygen of 0.086%, yield volume percentages of 0.62, 0.43, and 0.47 assuming FeO, Fe_2O_3, and Fe_3O_4 respectively. Since these volume percentages are less than observed, it is presumed that other compounds such as sulfides, phosphides, and other oxides are present. The photomicrograph of the etched specimen shows the grain diameter to be between 20 and 40 μ. The diamond pyramid hardness was 77. Previous investigators have attempted to correlate measurement results with the sum of total impurities present in their specimen. Interestingly, none of these analyses presented the oxygen content of the specimen, which is certainly not negligible in our specimen and possibly not in theirs. For comparison, Table 4 lists the summed carbon equivalent composition presented by Powell[10] for various studies. This table indicates that the Armco iron used in this study was not as pure as that used in previous studies.

Early in 1959 the Battelle Memorial Institute (BMI) initiated a round robin on the thermal conductivity of Armco Iron. Specimen material from one 7-ft length of annealed stock was supplied to cooperating laboratories. A point-counting technique was performed on a specimen of this stock and revealed the presence of 1.3 vol % of second phase. This evidence supports the above

Table 4. Carbon Equivalent Composition of Armco Iron Used in Various Thermal Conductivity Studies as Given by Powell[10]

Author	Equivalent Carbon Concentration[a]
Powell	0.041
Shelton	0.044
Mauner	0.042
Huttori	0.040
Armstrong and Dauphinee	0.070
Silverman	0.054
Lucks and Deem	0.036
Zegler and Nevitt	0.056
Laubitz	0.054
ORNL	0.06311 (min) 0.08276 (max) 0.1472 (max, including oxygen)

[a]Twelve times the sum of the ratio of the weight percent of each constituent to the atomic weight of the element.

proposition that the oxygen content is not negligible in other thermal conductivity samples of Armco iron.

The electrical conductivity measurements were obtained using a rod which was swaged from a 1 in. diameter to a diameter of 0.11 in. and then ground to 0.1000 ± 0.0001 in. This rod was annealed for 24 hr at 600°C in a vacuum of 5×10^{-7} torr prior to the measurements.

Thermal Conductivity Data

Two runs were made on iron in the range 100 to 1000°C. Run 1 was terminated at 819°C by an open circuit in the core-heater system. This was repaired, and run 2 was initiated to investigate four overlapping temperature ranges: 2A (100 to 925°C); 2B (700 to 930°C); 2C (925 to 1000°C); and 2D (752 to 925°C). Thermocouple instabilities were encountered between 840 and 950°C in run 2A, and the system was cooled to 700°C to determine the effect of these instabilities on the measured thermal conductivity. Isothermal cross checks between the electrical resistance of the Pt–10% Rh core heater with the specimen thermocouples indicated that a change of less than 2°C had occurred in the thermocouples. An increase in k of about 1% was observed between runs 2A and 2B. During run 2B, the thermocouples were more consistent internally than during run 2A in the same temperature region. The cause for this is not understood, but the general effect of enhanced thermocouple behavior at low temperatures after a high-temperature treatment (in this case 950°C) was observed during several of the UO_2 runs. Run 2B ended at 933°C, and the specimen was given an 8-hr anneal at 1050°C to achieve thermocouple stability in the region 925 to 1000°C. Thermal conductivity values at 933°C for runs 2B and 2C checked to within 1%, and the thermocouple performance during run 2C did not reveal any of the instabilities noted in run 2A; this justifies the 1050°C treatment. The final high-temperature run (run 2D) covered the range 750 to 925°C and was within 1% of runs 2B and 2C.

The data obtained in these runs are presented in Table E.1 of Appendix E and are plotted in Fig. 12. From 100 to 786°C the thermal conductivity of iron decreased with increasing temperature, and the data can be described to ±1.5% by two linear equations:

$$k = 0.7273 - 6.260 \times 10^{-4} t \quad (100 \leqq t \leqq 436°C), \tag{22}$$

$$k = 0.6554 - 4.609 \times 10^{-4} t \quad (436 \leqq t \leqq 786°C). \tag{23}$$

Thus the slope of the temperature dependence of the thermal conductivity of iron changes by 30% at about 436°C. The temperature dependence of k undergoes a drastic change at 786°C; in fact, k goes through a minimum in the range 780 to 790°C, and from 786 to 910°C the thermal conductivity increases linearly with increasing temperature. The data in this region may be represented by

$$k = 0.2703 + 2.854 \times 10^{-5} t \quad (786 \leqq t \leqq 910°C). \tag{24}$$

The thermal conductivity decreases 3 to 4% at the α-γ phase transformation (910°C). Above 910°C the thermal conductivity of γ-iron increases with increasing temperature to at least 1000°C, the

upper limit of the present experiment, and may be represented by the linear equation,

$$k = 0.1736 + 1.211 \times 10^{-4} t \quad (910 \leqq t \leqq 1000°C) . \tag{25}$$

Figure 13 is an expanded plot of the thermal conductivity data between 700 and 1000°C and shows that most of the data points lie in a ± 1.5% band around the equations.

A limited comparison of the results obtained on iron to 1000°C is made in Fig. 14. The four equations which fit the ORNL data to better than ±1.5% were used in their appropriate temperature ranges to obtain a difference plot with increasing temperature. Thus in Fig. 14 the zero

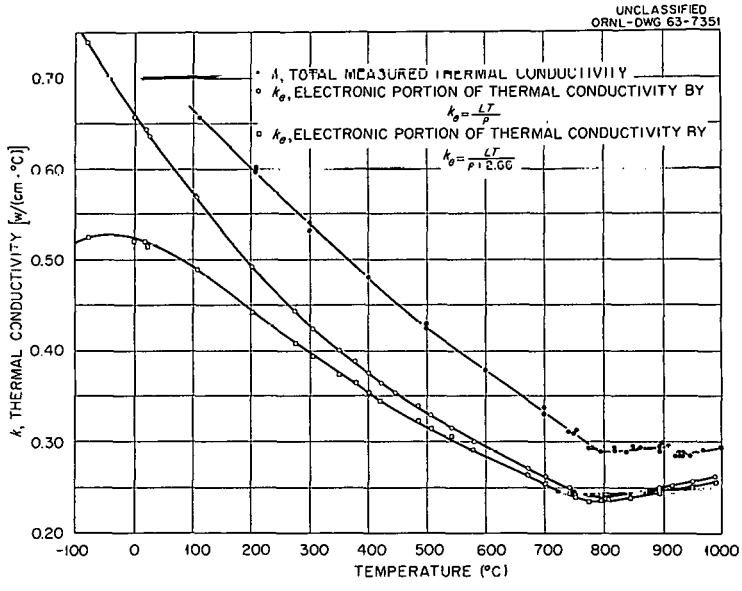

Fig. 12. Thermal Conductivity Results on Armco Iron from 100 to 1000°C and the Electronic Contribution Calculated by Two Methods.

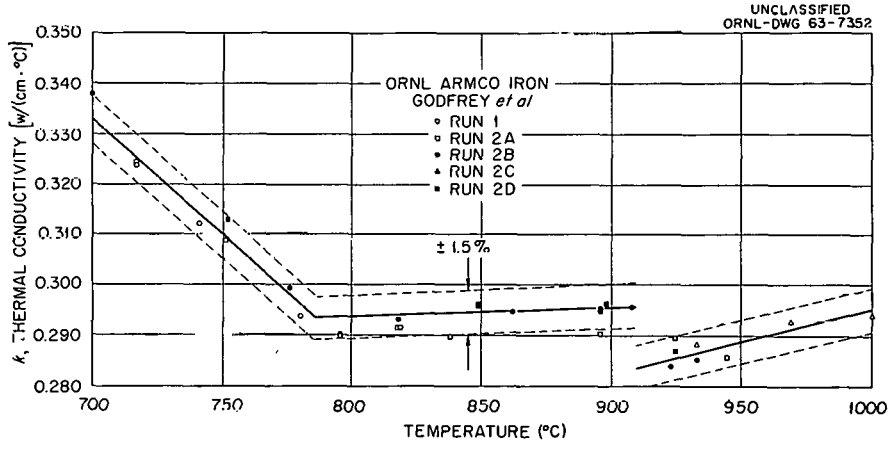

Fig. 13. ORNL Thermal Conductivity Results on Armco Iron from 700 to 1000°C.

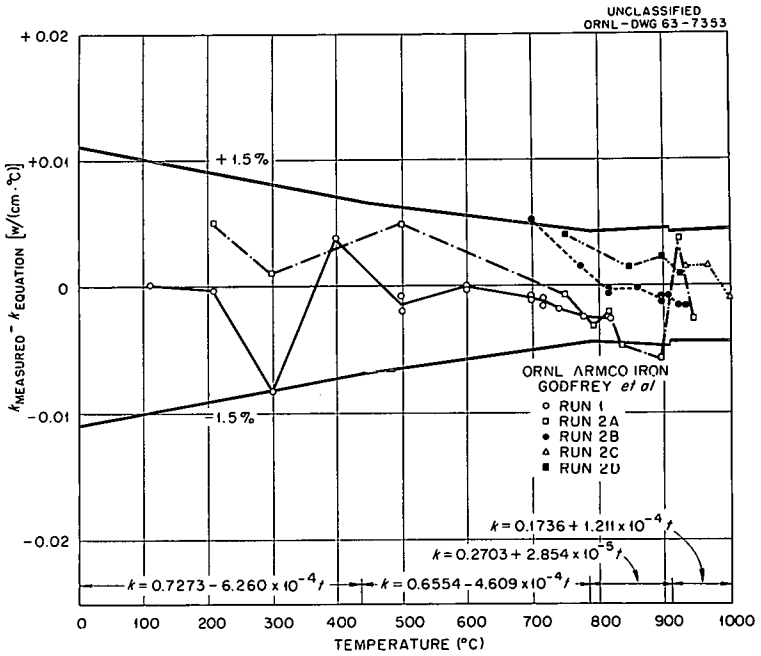

Fig. 14. Comparison of the ORNL Thermal Conductivity Results on Armco Iron to the Four Equations Which Span the Region 100 to 1000°C.

axis represents k vs t as determined by the equation indicated in the figure. A positive deviation represents a measured k greater than predicted by the equation, and a negative deviation represents a measured k less than predicted by the equation.

The deviation of the ORNL results from these equations shows the previously mentioned changes which occurred between the runs. Run 1 generated results to 820°C which, with one exception (the 300°C data), were well within 1% of the stated equations. The results of run 2A were nominally 1% above run 1 values and scattered above 820°C. The run 2A data above 820°C were not used in calculating Eqs. (24) and (25). Run 2B results were 1 to 2% above the results of run 1 and show a minimum scatter, reflecting the thermocouple stability induced by the 950°C anneal. Run 2C which was entirely in the γ-iron region and was preceded by the 1050°C anneal, yielded very consistent results. The results of run 2C were about 1% above the results of run 2B in the γ-iron region. The run 2D results were within 1% of all of the results of run 2B and are remarkably close to the run 2C results in the gamma region. Thus the measured results increased in value with increasing time above 700°C and reached stable values in runs 2C and 2D. The possibility of normalizing the results of run 2 to run 1 was considered but rejected at this stage of data presentation and interpretation. Naturally, all of the results are near the zero deviation line because these data were used to generate the comparison equations.

A similar comparison of the ORNL data and four sets of recent literature values on Armco iron are made in Fig. 15. Two of the four sets of data under comparison, those of the National Physical Laboratory (NPL)[36] and the National Research Council (NRC),[37] were obtained using specimens fabricated from the Armco iron circulated by BMI. The third data set was that presented by Powell[10] and termed by him to be the most probable value. The fourth set of data was obtained by Cody, Abeles, and Beers[38] of Radio Corporation of America Laboratories (RCA) on an Armco iron specimen by a thermal diffusivity technique. As will be discussed later, the RCA thermal conductivity values quoted here were obtained using a more recent set of specific heat data[39] than they originally used. The data plotted in Fig. 15 are presented in Table E.2. The NPL[36] and NRC[37] data were not corrected for thermal expansion, whereas the ORNL and RCA data were corrected.

---

[36]R. W. Powell *et al.*, "Armco Iron as a Thermal Conductivity Standard. Part II, New Determinations at the National Physical Laboratory," p 454 in *Progress in International Research on Thermodynamic and Transport Properties* (ed. by J. F. Masi and D. H. Tsai), The American Society of Mechanical Engineers and Academic Press, New York, 1962.

[37]M. J. Laubitz, "Thermal and Electrical Properties of Armco Iron at High Temperatures," *Can. J. Phys.* 38(7), 887 (1960).

[38]G. D. Cody, B. Abeles, and D. S. Beers, "Thermal Diffusivity of Armco Iron," *Trans. Met. Soc. AIME* 221(2), 25 (1961).

[39]D. L. McElroy, "The Application of Dynamic Adiabatic Calorimetry to the Iron–Iron Carbide System," Ph.D. dissertation, University of Tennessee (August 1957).

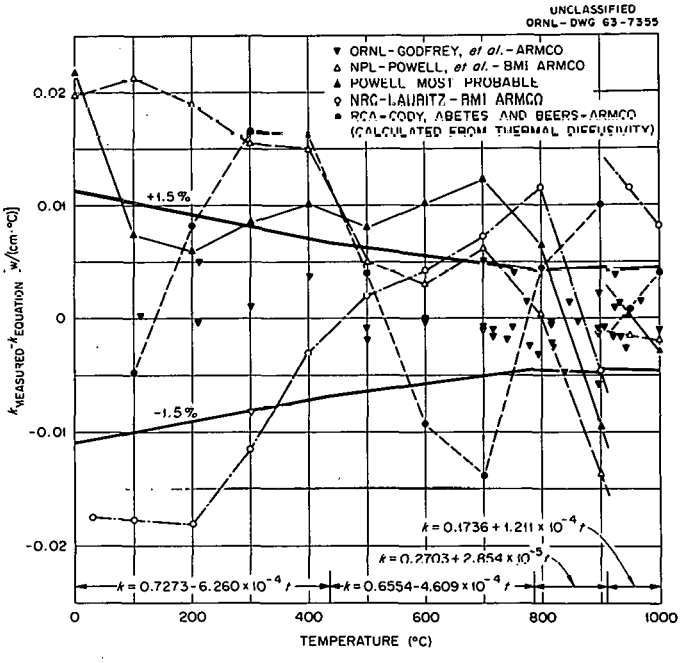

Fig. 15(*a*). Comparison of the Thermal Conductivity of Armco Iron of Various Studies to the Four Equations That Represent the ORNL Results from 0 to 1000°C.

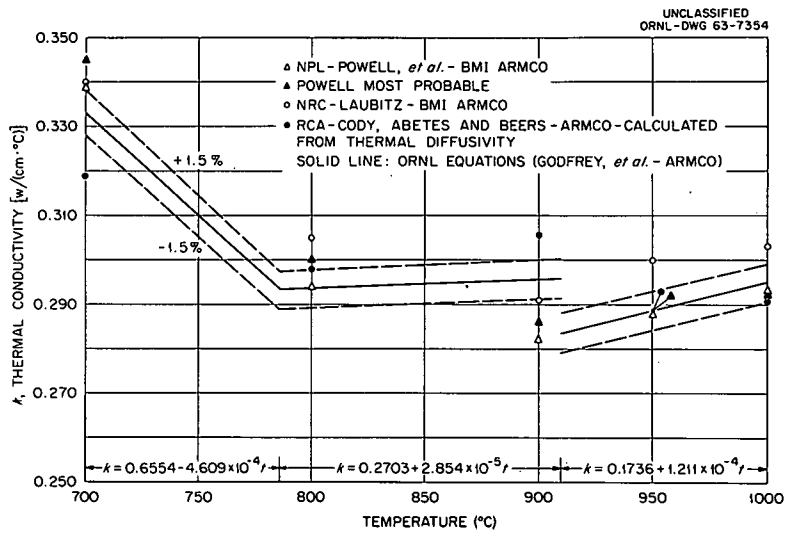

Fig. 15(*b*). Comparison of the Thermal Conductivity of Armco Iron of Various Studies to the Three Equations That Represent the ORNL Results from 700 to 1000°C.

On the BMI samples the NPL results are 3% higher than the equations to 400°C. On the other hand, the NRC values* are 3% below the ORNL equations to 200°C, approach the equations from 200 to 500°C, and deviate from the equations from 500 to 900°C. Powell's most probable values[10] are 1 to 2% above the equations from 100 to 800°C but deviate at 0 and 900°C by as much as 3%. From 900 to 1000°C the NPL results and Powell's most probable values are within 1.5% of the equation, whereas the NRC results are about 3% high. The RCA data scatter in a ±3% band around the equations from 100 to 900°C but are in good agreement from 900 to 1000°C with the equations. Only the RCA and ORNL data show a decrease in thermal conductivity at the α-γ transformation; however, the RCA data indicate a 6 to 7% change, while the ORNL values indicate a 4% change. Not included in Fig. 15, but of significance is the data of Claussen,[40] who also observed a decrease of k on passing through the α-γ transition; this decrease amounted to a 15 to 20% change at pressures of 9000 atm. Perhaps the most striking observation of this comparison is that four different laboratories using four different methods of measurement obtained results within ±3% over the 100 to 1000°C range.

Electrical Resistivity Data

Electrical resistivity measurements were made on a rod specimen 12 in. long and 0.1 in. in diameter. For temperatures above room temperature the specimen was directly heated by a direct current in a vacuum of 5×10^{-7} torr. The center 6 in. of the rod was instrumented with

*Dr. Laubitz has informed us that the low-temperature NRC data are plotted about 1% lower than they should be. This is due to the fact that a small correction was overlooked when the data was reported in ref 37.

[40]W. F. Claussen, "Detection of the α-γ Iron Phase Transformation by Differential Thermal Conductivity Analysis, *Rev. Sci. Instr.* 31(8), 878 (1960).

seven 0.005-in.-diam Pt vs Pt–10% Rh thermocouples spaced at 1-in. intervals. The thermocouples were tweezer-welded to the rod so that the junction was made through the iron specimen. The 0.005-in.-diam Pt–10% Rh and Pt wires were welded to 0.020-in.-diam wires a few inches away from the specimen, and these larger wires extended out of the vacuum chamber through epoxy resin seals to an ice-bath cold well similar to the one described for the radial heat flow apparatus. The thermocouple emf's were read using an L&N type K-3 potentiometer. The current through the specimen was produced by a PRL 50-amp-dc power supply model CM-03-5L-CC and was measured by reading the potential drop across a series-connected 0.01-ohm L&N standard resistor, model No. 4361, with the L&N type K-3 potentiometer. For temperatures below room temperature the specimen was immersed in three baths: ice and water (0°C); dry ice and alcohol (–78.9°C); and liquid nitrogen (–196°C).

The resistivity was obtained by measuring the current and the corresponding potential drop between the Pt–10% Rh legs of a set of adjacent thermocouples at a given temperature. The set of thermocouples chosen were near the center of the rod so that both thermocouples were at essentially the same temperature. Readings were made at each temperature with the current in one direction and then the other so that pickup errors in the thermocouples could be eliminated. The resistivity was calculated using the formula

$$\rho = \frac{\Delta \bar{V}}{\bar{I}} \frac{A^*}{L^*} \left[1 + \alpha_L (t - 23)\right], \tag{26}$$

where

$\Delta \bar{V}$ is the average potential drop between the Pt–10% Rh legs for the current in the forward and reverse directions,

$\bar{I}$ is the average of the forward and reversed currents,

L^* is the distance between the Pt–10% Rh wires,

A^* is the cross-sectional area of the rod,

t is the temperature in °C,

α_L is the expansion coefficient, 13.5×10^{-6} per °C (ref 37).

The maximum determinate error in ρ due to measurement uncertainties in the quantities of Eq. (26) was estimated (as shown in Appendix F) to be ±1.3%, with a most probable value of ±1.0% if the errors behave randomly.

Using this technique the resistivity vs temperature curve was found to be concave upward to about 750°C, where an inflection occurs and the resistivity increases approximately linearly above 900°C. This is the usual shape of the electrical resistivity curve for ferromagnetic materials near the Curie temperature. The data were fit by least-mean-squares criteria to within 2% in the range 194 to 780°K by a cubic equation

$$\begin{aligned} \rho &= C_1 + C_2 T + C_3 T^3 , \\ &= -1.43 + 3.85 \times 10^{-2} T + 6.30 \times 10^{-8} T^3 , \end{aligned} \tag{27}$$

where ρ is in μohm-cm, and T is absolute Kelvin temperature. Above 800°C the resistivity could

be expressed by the linear relation

$$\rho = 74.9 + 3.38 \times 10^{-2} T \, . \tag{28}$$

Following the electrical resistivity measurements, the distances between thermocouples and the diameter of the rod were remeasured and were found to be the same as originally even though the specimen had been cycled through the α-γ transformation several times. It was impossible to so examine the thermal conductivity specimen because the disks of the stack became welded together during the experiment.

Values of ρ obtained between –196°C and 1000°C are given in Table G.1 of Appendix G. Smoothed values are presented in Table 5 at 50°C increments together with values of Powell *et al.*[36] and Laubitz.[37] The data of the other laboratories as well as the ORNL data have been corrected for thermal expansion using 13.5×10^{-6}/°C as the thermal expansion coefficient throughout the entire temperature range even though iron undergoes a linear contraction

Table 5. Smoothed Electrical Resistivity Values for Armco Iron

ORNL		NPL		NRC	
Temperature (°C)	ρ (μohm-cm)	ρ (μohm-cm)	Deviation (%)	ρ (μohm-cm)	Deviation (%)
−150	3.2	3.3	+3.0		
−100	5.3	5.3	0.0		
−50	7.6	7.5	−1.3		
0	10.2	10.0		10.4	
50	12.6	12.5	−0.8		
100	15.9	15.6	−1.9	15.6	−1.9
150	19.4	19.1	−1.6		
200	23.3	23.1	−0.9	23.0	−1.3
250	27.8	27.1	−2.6		
300	32.7	31.3	−4.4	32.1	−1.9
350	38.2	36.5	−4.6		
400	44.0	42.0	−4.7	43.1	−2.1
450	50.3	47.7	−5.3		
500	56.7	54.4	−4.2	56.1	−1.1
550	64.1	61.4	−4.3		
600	72.0	69.4	−3.7	70.9	−1.5
650	80.7	77.8	−3.7		
700	90.2	87.0	−3.6	88.8	−2.5
750	101.2	97.8	−3.4		
800	108.7	106.4	−2.1	107.1	−1.5
850	112.4	111.1	−1.2		
900	114.5	113.8	−0.7	113.4	−1.0
950	116.2	115.6	−0.5		
1000	117.7	117.4	−0.3	116.8	−0.8

of about 0.3% (ref 37) at the α-γ transition at 910°C. The percent deviation of the data is also shown in this table. It is seen that, except for the value at 700°C, the ORNL data agree with that of NRC[37] to within 2%, which is within the sum of the estimated accuracies of the measurements. The disagreement with NPL[36] was less than 2% from −150 to 200°C and again from 800 to 1000°C, but the deviation in the range from 200 to 800°C was as much as 5%, which is well outside the estimated accuracies of the methods used in the two laboratories. The reason for the discrepancies may be due to specimen differences or to some unassessed inaccuracies in the measurement techniques. It is interesting to note that the discrepancies are greatest in the temperature range where the resistivity changes most rapidly, indicating that temperature measurement errors may be present. Powell *et al.*[36] report a sudden drop in the electrical resistivity at the α-γ transition of about 1.6 μohm-cm. Such a change, if it occurred, was <1 μohm-cm for the ORNL specimen but insufficient data were taken around the transformation temperature to establish the effect accurately.

DISCUSSION OF THE RESULTS ON IRON

Discussion of k_e and k_L

For the purpose of discussion it will be assumed that the thermal conductivity of iron may be expressed as

$$k = k_e + k_L \,, \tag{29}$$

where k_e is the contribution due to transport of heat by electrons, and k_L is the contribution due to transport by heat by phonons. Actually the two mechanisms are coupled, although it is generally assumed that the coupling is weak. The electronic portion, k_e, can be calculated from the electrical resistivity data using the theoretical Wiedemann-Franz-Lorenz constant L by the equation

$$\frac{k_e \rho}{T} = L = 2.45 \times 10^{-8} \text{ w-ohm/(°K)}^2 \,. \tag{30}$$

The validity of this relation depends on the relaxation time for electrons under the disturbance of an electric field being the same as that for the disturbance caused by a thermal gradient. It is also necessary that the relaxation time and the rate of change of the energy of the electron states with change of the wave vector be slowly changing functions of the electron energy near the Fermi surface. These conditions should be fulfilled for a one-band metal at high temperatures. There is some doubt, however, whether the relation is valid for transition metals where the *s* and *d* bands may overlap.

Recently, Backlund[41] suggested that a modified Wiedemann-Franz-Lorenz type relation, originally proposed by Linde,[42] should be applied to iron. This relation is

$$k_e = \frac{LT}{\rho + \rho_0} . \tag{31}$$

The constant ρ_0 was obtained by Backlund for "pure" iron by fitting his data together with those of Pallister[43] in the temperature range 195 to 373°K to a cubic equation of the same form as Eq. (27), where ρ_0 is the absolute value of the constant term C_1 in this equation. In his paper Backlund indicates three different values of ρ_0 (+2.4, 2.6, and 2.66 μohm-Cm), but evidently 2.66 is the value which he considers to correspond to pure iron. Since impurities contribute to C_1, the apparent value of ρ_0 will be changed by impurities. This evidently accounted for the various values cited. This impurity effect is shown in Table 6. The values of the three constants in the cubic equation for ρ are given as obtained by least-mean-squares fitting of the ORNL data and those of Powell *et al.*[36] The values of C_1 for Armco iron (an impure iron) are considerably larger than Backlund's value of $-\rho_0$. The table also shows that the value of the coefficients vary, depending on the temperature range over which the fit was made.

Backlund contends that the cubic term C_3T^3 represents a spin scattering contribution which should become constant above the Curie temperature. Therefore the slope of Eq. (28) should be the same as the constant C_2 of Eq. (27). Examination of Table 6 shows that the values of C_2 agree well with the value of the slope, 3.38×10^{-2} μohm-cm/°K in Eq. (28), which supports Backlund's contention.

---

[41] N. G. Backlund, "An Experimental Investigation of the Electrical and Thermal Conductivity of Iron and Some Dilute Iron Alloys at Temperatures Above 100°K," *J. Phys. Chem. Solids* 20 (1/2), 1–16 (1961).

[42] J. O. Linde, "An Investigation of the Validity of the Wiedemann-Franz-Lorenz Law," *Arkiv. Fysik* 4(38), 541 (1951).

[43] P. R. Pallister, "The Specific Heat and Resistivity of High Purity Iron Up to 1250°C," *J. Iron Steel Inst.* 161, 87 (1949).

Table 6. Constants for a Cubic Fit of the Electrical Resistivity Data for Armco Iron Where $\rho = C_1 + C_2T + C_3T^3$

Author	Temperature Range (°K)	C_1 (μohm-cm)	$C_2 \times 10^2$ (μohm-cm/°K)	$C_3 \times 10^8$ (μohm-cm/°K^3)
ORNL	195–380	−1.69	3.88	6.03
	195–780	−1.43	3.85	6.30
Powell[36]	173–373	−1.34	3.65	6.33
	173–723	−1.93	3.98	5.58
Backlund[41] and Pallister[43]	195–373	−2.4	3.65	6.4[a]

[a] This value appeared as 64×10^{-8} in ref 41, evidently by misprint.

Calculation of k_e and k_L

Despite the uncertainty in ρ_0, k_e was calculated using Eq. (31). A value of ρ_0 of 2.7 μohm-cm was used. The values of k are plotted in Fig. 12 along with k_e calculated by Eqs. (30) and (31). Figure 16 shows k_L obtained as the difference $k - k_e$ using both values of k_e. With the conventional Wiedemann-Franz-Lorenz relation, k_e accounts for 80% or more of the total thermal conductivity and therefore largely controls the temperature dependence of the thermal conductivity. This is also true at high temperatures for k_e calculated by Eq. (31) but at 100°C is only 73% of k and displays a maximum near 250°K. Using the usual Wiedemann-Franz-Lorenz approach, k_L peaks at about 300°C, which is considerably above the Debye temperature of 147°C (ref 44). Generally, the lattice conductivity peaks at temperatures considerably

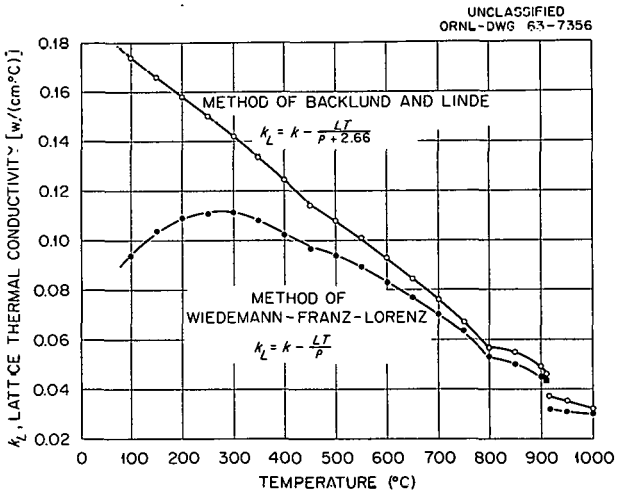

Fig. 16. Lattice Thermal Conductivity of Armco Iron as a Function of Temperature, Calculated by Two Methods.

below the Debye temperature. However, we have already seen that this rule does not apply to UO_2 because of a low-temperature antiferromagnetic-paramagnetic transformation. Some similar phenomenon of magnetic origin may explain the behavior of iron. Using the Backlund modified Wiedemann-Franz-Lorenz approach, one eliminates the high-temperature peak in k_L. However, as can be seen from Fig. 12, the Backlund k_e has a peak at about 250°K, which seems just as unreasonable as the peak in k_L obtained using the Wiedemann-Franz-Lorenz relation. At the present state of the theory of thermal conductivity, it is not at all obvious which of the approaches for calculating k_e and k_L approaches closest to reality.

---

[44] F. Seitz, *The Modern Theory of Solids*, p 110, McGraw-Hill, New York, 1940.

Decrease in k at 910°C

The 4% decrease at the α-γ transition is not predicted by the k_e's. In fact, the electrical resistivity decrease at the transition temperature reported by Powell *et al.*[36] should be reflected by an increase in k rather than the decrease observed. The change in k at 910°C must be due to a decrease in the lattice portion of the conductivity as shown in Fig. 15 and is tied to the fact that a change from body-centered cubic to face-centered cubic structure causes an appreciable modification of the phonon distribution. Cody, Abeles, and Beers[38] have pointed out that if Eq. (9) applies to k_L of iron at high temperatures, then the decrease in the Debye temperature upon going from α to γ phases (which is consistent with existing heat capacity data for the phases) can explain the drop in k_L. At 910°C k_L amounted to ~15% of the total thermal conductivity, and the observed 3 to 4% decrease in k can be explained by a 10% decrease in the Debye temperature. However, it should be pointed out that if k_L obeys Eq. (9), it should have a $1/T$ temperature dependence, which it does not have regardless of the method one uses to calculate k_e. The temperature dependence of k_L is closer to a $1/T$ relation using the Backlund-Linde method.

Slope Change of k at 780°C

The minimum in k just above the Curie temperature is reflected by both k_e's and is apparently due to the effect of the changed magnetic properties on the electronic portion of the thermal conductivity since k_e also changes slope, as shown in Fig. 12. It should be pointed out that no

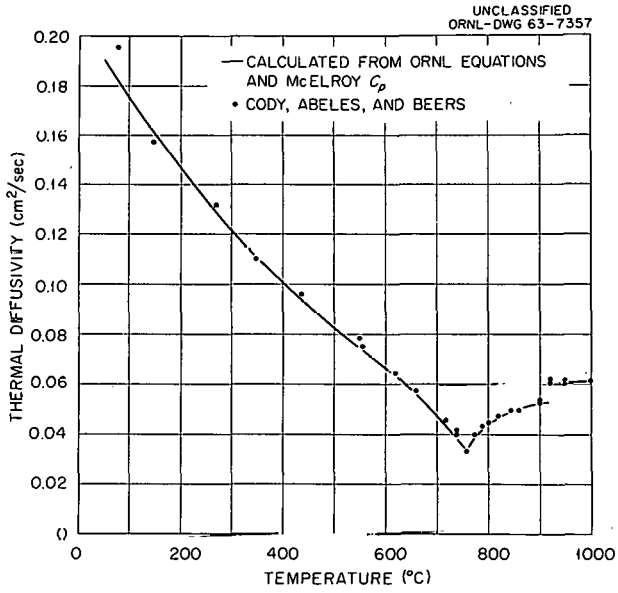

Fig. 17. Thermal Diffusivity of Armco Iron Calculated from ORNL Thermal Conductivity Data and Heat Capacity Data of McElroy[39] and Compared with the Thermal Diffusivity Data of Cody, Abeles, and Beers.[38]

break or discontinuity in the data of the type reported by Cody, Abeles, and Beers[38] at the magnetic transformation temperature 768°C was observed. Data were taken in this temperature region, as shown in Fig. 13, and the average Δt between inside and outside thermocouples was only 3 to 4°C; therefore any discontinuity or drastic change in slope should have been detected. This points out the difficulty of obtaining accurate thermal conductivity values from thermal diffusivity measurements in a temperature range where the heat capacity of the specimen is changing rapidly with temperature.

The thermal diffusivity data of Cody, Abeles, and Beers[38] is plotted in Fig. 17, and these data are compared with thermal diffusivities calculated using the ORNL thermal conductivity values and McElroy's values[39] for the specific heat of iron. It is seen that the agreement is excellent over the whole temperature range, including the region near the Curie point. This clearly shows the need for very good heat capacity values when the thermal conductivity is calculated from thermal diffusivity measurements.

Slope Change of k at 436°C

The break in k at 436°C may be an impurity or magnetic effect since iron itself does not have a solid-state phase change in this region. It is interesting to note that Laubitz[37] has reported a minimum in the thermoelectric power of Armco iron at about this temperature.

Correlation of k at 100°C with Impurity Content

Powell[10] gives a linear correlation between measured k values at 100°C and the equivalent carbon content of all reported impurities; this correlation predicts a thermal conductivity of 0.694 w cm^{-1} $°C^{-1}$ for pure iron. The ORNL data fit this correlation if oxygen is excluded; however, inclusion of oxygen would lead to a prediction of 0.726 w cm^{-1} $°C^{-1}$ for pure iron using a parallel straight line. As was previously stated, our calculations indicated that sulfides, phosphides, and oxides were also present as a second phase. Theory dictates that only the impurities in solution should be included in a correlation such as Powell's. However, he has included sulfur and phosphorus in his correlation. If it is assumed that the second phase has a thermal conductivity smaller than that of the iron, its effect on k should be a reduction which is no greater than the volume percent of the phase (in this case, <1%). The effect of dissolved impurities should be much larger than, but in the same direction as that of the second phase. The point to be stressed is that one must know not only the composition of the specimen but also the physical state in which the impurities are found in order to assess the effects of these impurities on thermal and electrical conductivity.

CONCLUSIONS

The radial heat flow apparatus was shown to give absolute thermal conductivity results with a probable accuracy of ±1.5% and a repeatability of 0.1% from 100 to 1100°C on both a low-conductivity semiconductor, UO_2, and a high-conductivity metal, Armco iron. The upper temperature limit was imposed by Pt vs Pt–10% Rh thermocouple instability although the apparatus was structurally sound and operable to at least 1400°C. The lower temperature limit was imposed by present design, but tests have shown that with only slight modification much lower temperatures can be obtained.

The ORNL results on polycrystalline UO_2 showed:

1. The thermal resistance, $1/k$, is linear between 200 and 1000°C with a characteristic slope of 0.0223 cm/w from which a Debye temperature of 216°C was derived. Below 1000°C, heat is transported by phonons.
2. The intercept of the linear portion of the thermal resistance is sensitive to impurity changes (i.e., stoichiometry changes).
3. The thermal conductivity displays a maximum near room temperature which can be associated with the behavior of the specific heat.
4. Between 1000 and 1100°C the negative deviation of the thermal resistance of 1 to 3% from the extrapolation of the linear portion was probably due to a compositional change in the material; however, the possibility of an electronic or radiation contribution to the thermal conductivity is not ruled out.

The ORNL results on Armco iron showed:

1. The thermal conductivity of polycrystalline Armco iron could be represented to within ±1.5% from 100 to 1000°C by the four linear relations:

$$k = 0.7273 - 6.260 \times 10^{-4} t \qquad (100 \leqq t \leqq 436°C),$$
$$k = 0.6554 - 4.609 \times 10^{-4} t \qquad (436 \leqq t \leqq 786°C),$$
$$k = 0.2703 + 2.854 \times 10^{-5} t \qquad (786 \leqq t \leqq 910°C),$$
$$k = 0.1736 + 1.211 \times 10^{-4} t \qquad (910 \leqq t \leqq 1000°C).$$

   The values given by these equations are within ±3% of the best numbers available from the literature.
2. The cause for the change in slope at 436°C is not known, but it may be related to the fact that Armco iron has a minimum in the Seebeck coefficient at about this temperature.
3. The minimum in the thermal conductivity at 780°C, just above the Curie temperature, reflects the change in magnetic properties of the material.
4. Electrical resistivity measurements showed that about 80% of the thermal conductivity can be attributed to electronic conduction; therefore this contribution largely controls the temperature dependence of the thermal conductivity.
5. The 4% drop in the thermal conductivity observed at the α-γ transformation is attributed to a 30% drop in the lattice portion of the thermal conductivity.

In this work we have made an intensive effort to obtain the best possible thermal conductivity measurements. We believe that the results show some interesting and important behaviors which could not have been detected without careful measurements, for example, the 4% drop in k at the

α-γ transformation in iron. It goes without saying that, having once invested the price of development of careful techniques, we are now in a position to make good measurements in the future routinely with as little effort as would be required for far less precise methods.

RECOMMENDATIONS

A report such as the foregoing is most worthwhile if it accomplishes the goals of the research, reveals new and useful information, points out gaps in current knowledge of science and technology, and indicates profitable routes for future work to pursue. It is in this light that we believe this research was worthwhile. As the Conclusions point out, a useful, accurate, and absolute device was developed. New and confirmatory information was obtained on two most different and interesting materials which had previously been extensively investigated. The information obtained is not in itself complete, but it should assist future research of these and other materials.

Based on the reported results, we recommend the following as profitable avenues for future research.

1. Development work on the radial heat flow apparatus should continue with the simultaneous goals of (*a*) expanding the existing temperature range of operation; (*b*) reducing the specimen size requirements; (c) maintaining and improving the accuracy and reproducibility of the data; (*d*) reducing the time of measurement; and (e) simplifying the operation of the equipment.

2. Accurate thermal conductivity measurements on both polycrystalline UO_2 and Armco iron to higher temperatures should be continued, as well as simultaneous measurement of other thermophysical properties such as electrical resistivity, Seebeck coefficient, specitic heat, and infrared absorption coefficients. Specimen variables worthy of consideration include purity, grain size, porosity, and thermal and mechanical treatments.

3. The accuracy achieved in this apparatus warrants extension of it to measurements on other solids, including those materials classified as scientifically interesting, to study phenomological effects (such as the various heat transport mechanisms); those materials which can be classified as new and as possessing unknown thermal properties; those classified as thermal conductivity reference standards to allow more meaningful measurements by investigators using comparative methods; and those classified as engineering materials whose thermal properties are critical to obtain efficient devices. Generally the specimen size requirements for this apparatus are a trivial problem in the latter two cases, and technological advances in material processes are making this less of a problem in the former two cases.

4. The sophistication of any quantitative data treatment or theoretical analysis is limited by the accuracy of the measurements of numerous physical properties, and this is the main product a careful and critical experimentalist can supply to a theoretician. The experimentalist is often requested for an answer regardless of accuracy. Undoubtedly, such requests must be

honored; but when they are so honored, the result is that the experimentalist is reduced to a well-paid technician, the information useful to a theoretician is drastically reduced, and the entire measurement must normally be repeated within a few years using careful procedures. This is not a recommendation for the experimentalist to reduce the quantity level of his work but to define and increase the quality of his work to allow meaningful progress to be obtained in the physical properties field. One particular aspect which would be of invaluable aid is the tabulation of raw data to avoid meaningless cross comparisons which are based on interpolations of smooth curves drawn on postage-stamp-size graphs!

THIS PAGE

WAS INTENTIONALLY

LEFT BLANK

Appendix A

THERMOCOUPLE LEAD-THROUGHS

In order to make the apparatus more versatile, a demountable thermocouple lead-through was devised which would accommodate many thermocouple wires using minimum space. Design criteria were (1) ease of assembly, (2) continuity of thermocouple wire without the use of a second metal in the circuit, (3) vacuum tightness, and (4) mechanical strength. The basic design of the lead-through is shown in Fig. A.1. The pieces were machined from brass stock and tubing. The short pieces of $\frac{1}{16}$-in.-diam two-hole refractory insulators were held in place with household cement. The thermocouple wires were threaded through the insulators, and the cavity was filled with a low-vapor-pressure epoxy resin. The vacuum seal to the baseplate was effected with an O-ring. Sealing pressure was supplied by a flat steel washer and four machine screws threaded into blind holes in the baseplate. The lead-through proved to be entirely satisfactory in all respects.

The use of a taper seal on the O-ring was dictated by the fact that the lead-through holes in the baseplate of the apparatus had been machined previously with the recessed shoulder for another type of seal. Had it been possible to use the more desirable flat O-ring seal, the brass body of the lead-through would have been made larger to accommodate the O-ring groove and the holes for the clamping screws, thus eliminating the steel washer.

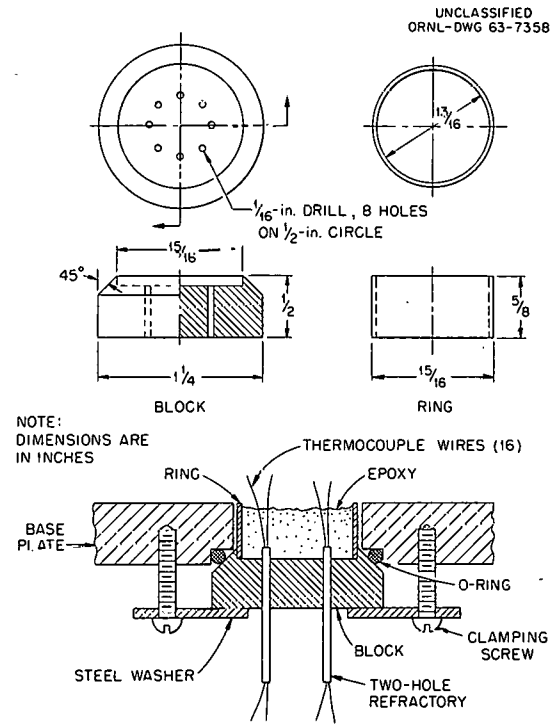

Fig. A.1. Thermocouple Lead-Through Design.

A second type of thermocouple lead-through was used to accommodate several thermocouples which were added to the system at a later date. This lead-through employed the body of a $\frac{1}{4}$-in. male-pipe-to-tube brass fitting. The thermocouple wires passed through two-hole refractory tubes which extended part way through the fitting. After the openings on one end were sealed with putty, the center cavity was filled with epoxy resin. The brass fitting was then screwed into a tapped hole in the baseplate with Teflon tape as the thread sealant. This lead-through also satisfied the criteria enumerated previously.

Appendix B

DETERMINABLE ERRORS FOR THE RADIAL HEAT FLOW APPARATUS

Equations (1) and (3) may be rewritten as

$$k = \frac{SQ\ (\ln r_2 - \ln r_1)}{2\pi L^* [(\bar{V}_1 - \bar{V}_2)_{data} - (\bar{V}_1 - \bar{V}_2)_{iso}]}, \tag{B.1}$$

where $\bar{V}_2$ is the average reading of the thermocouples at radius r_2, $\bar{V}_1$ is the average at r_1, and S is the thermocouple sensitivity. The uncertainty in k (Δk), due to uncertainties in the quantities on the right side of Eq. (B.1), may be determined by partial differentiation, which yields

$$|\Delta k| = \left|\frac{\partial k}{\partial Q}\Delta Q\right| + \left|\frac{\partial k}{\partial S}\Delta S\right| + \left|\frac{\partial k}{\partial L^*}\Delta L^*\right| + \left|\frac{\partial k}{\partial r_2}\Delta r_2\right| + \left|\frac{\partial k}{\partial r_1}\Delta r_1\right|$$
$$+ \left|\frac{\partial k}{\partial(\bar{V}_1 - \bar{V}_2)_{data}}\Delta(\bar{V}_1 - \bar{V}_2)_{data}\right| + \left|\frac{\partial k}{\partial(\bar{V}_1 - \bar{V}_2)_{iso}}\Delta(\bar{V}_1 - \bar{V}_2)_{iso}\right| . \tag{B.2}$$

Taking the indicated partials and dividing the result by Eq. (B.1) yields

$$\epsilon_k = \frac{|\Delta k|}{k} = \frac{|\Delta Q|}{Q} + \frac{|\Delta S|}{S} + \frac{|\Delta L^*|}{L^*} + \frac{|\Delta r_2|}{r_2 \ln (r_2/r_1)} + \frac{|\Delta r_1|}{r_1 \ln (r_2/r_1)}$$
$$+ \frac{|\Delta(\bar{V}_1 - \bar{V}_2)_{data}|}{(\bar{V}_1 - \bar{V}_2)_{data} - (\bar{V}_1 - \bar{V}_2)_{iso}} + \frac{|\Delta(\bar{V}_1 - \bar{V}_2)_{iso}|}{(\bar{V}_1 - \bar{V}_2)_{data} - (\bar{V}_1 - \bar{V}_2)_{iso}} = \Sigma \epsilon_i . \tag{B.3}$$

where ϵ_k is the fractional uncertainty in k, and ϵ_i is the fractional uncertainties in the quantities on the right-hand side of Eq. (B.1). Substitution of the proper values yields the maximum value of the fractional uncertainty in k. These values are given in Table B.1 for the iron and UO_2 specimens.

If the measurement errors are assumed to be random, the "most probable" value of the error due to these measurements may be assessed as

$$\epsilon_{\substack{most \\ probable}} = (\Sigma \epsilon_i^2)^{1/2} . \tag{B.4}$$

It must also be considered that for a given measuring plane, there are several thermocouples, n, at both r_1 and r_2, so that the probable error in r_1 and r_2 is the value shown in Eq. (B.3) reduced by a factor $1/\sqrt{n}$. Similarly there are m measuring planes so that the most probable error for the average value of all the planes is the value of $\epsilon_{most\ probable}$ from Eq. (B.4) reduced by a factor $1/\sqrt{m}$. From the values in Table B.1, after multiplying the values of $|\Delta r_1|/[r_1 \ln (r_2/r_1)]$ and $|\Delta r_2|/[r_2 \ln (r_2/r_1)]$ by $1/\sqrt{2}$ for UO_2 and $1/\sqrt{3}$ for iron, one obtains $\epsilon_{most\ probable}$ for UO_2 of 0.0164 and 0.0176 for iron. These values are then multiplied by $1/\sqrt{3}$ and $1/\sqrt{2}$, respectively, to allow for three measuring planes for UO_2 and two measuring planes for iron to obtain $\epsilon_{most\ probable}$ values of 0.0095 for UO_2 and 0.0125 for iron.

Table B.1. Calculation of Determinable Errors

	UO_2	Armco Iron
$\frac{\lvert\Delta Q\rvert}{Q}$	0.00056	0.00056
$\frac{\lvert\Delta L^*\rvert}{L^*}$	0.0067	0.0067
$\frac{\lvert\Delta r_2\rvert}{r_2 \ln r_2/r_1}$	0.0062	0.0095
$\frac{\lvert\Delta r_1\rvert}{r_1 \ln r_2/r_1}$	0.0188	0.0249
$\frac{\lvert\Delta s\rvert}{s}$	0.005	0.005
$\frac{\lvert\Delta(\bar{V}_1 - \bar{V}_2)_{data}\rvert}{(\bar{V}_1 - \bar{V}_2)_{data} - (\bar{V}_1 - \bar{V}_2)_{iso}}$	~0.00020	~0.0010
$\frac{\lvert\Delta(\bar{V}_1 - \bar{V}_2)_{iso}\rvert}{(\bar{V}_1 - \bar{V}_2)_{data} - (\bar{V}_1 - \bar{V}_2)_{iso}}$	~0.00020	~0.0010
Total	0.038	0.049

Appendix C

THERMOCOUPLE-IMMERSION-DEPTH TEST

An auxiliary experiment was performed to assess the possible error due to the fairly shallow ($\frac{3}{8}$ in.) thermocouple immersion in the UO_2 specimen. The test consisted in probing, with several thermocouple configurations, the length of a 0.063-in.-diam hole along the axis of a 4-in.-diam 2-in.-long copper cylinder. The cylinder was heated on the face opposite the thermocouple entry hole by a laboratory hot plate to temperatures from 27 to 120°C, while the other face freely radiated. The cylindrical surface was insulated to promote axial heat flow. Auxiliary thermocouple probes perpendicular to the cylinder axis established that the copper block maintained an axial gradient less than 0.1 μv/in. (0.02°C/in.).

This test approximated the conditions that exist in the radial heat flow apparatus in that the copper block represents the isothermal zone of the thermocouple well in the specimen, and the copper-air interface temperature drop represents the gradient imposed on the thermocouple as it extends from the well radially to the surface of the specimen. However, the test was overly severe in that the copper-air interface gradient was much greater than actually exists in the apparatus and that the conducting gas (air) in the thermocouple well had a much lower conductivity than helium. Also, these low-temperature tests were stringent in that radiative heat transfer to the thermocouple was negligible.

All of the thermocouple configurations tested employed 0.010-in.-diam Pt vs Pt–10% Rh wire insulated in (1) unbroken two-hole 0.0625-in.-diam Al_2O_3 tubing; (2) the same tubing broken into $\frac{1}{8}$-in.-long pieces; (3) two 0.030-in.-diam one-hole Degussa Al23 tubes; (4) the same as (3) except broken into $\frac{1}{8}$-in.-long pieces; and (5) the broken Degussa pieces of (4) with the thermocouple junction capped by a $\frac{1}{16}$-in.-long $\frac{1}{16}$-in.-diam one-hole Al_2O_3 tube as is used in the radial heat flow apparatus.

Results typical of those obtained are shown in Fig. C.1. The thermocouple insulated with the broken Degussa pieces showed a 50% smaller error than the one with unbroken tubes at an immersion of $\frac{3}{8}$ in., while the addition of the end cap reduced the error by an additional 50%. Figure C.2 shows a summary of all results expressed as the error for a $\frac{3}{8}$-in. immersion depth. These results are entirely consistent with expectations and show that for the broken-Degussa-with-end-cap configuration, the error is 0.04 μv/(°C ΔT) or about 0.007 μv/(μvΔE) at these temperatures. The error that would appear in a thermal conductivity measurement in the radial heat flow apparatus would be the difference between the errors for the two radial positions with their different radial gradients. In the copper block experiment, the gradient exists over a very short distance, certainly no more than 0.1 in. into the air. By analysis of the gradients over comparable distances at the two radial positions in the radial heat flow apparatus, it may be shown that the error introduced in k is $<0.1\%$ for a $\frac{3}{8}$-in. immersion depth and is independent of specimen thermal conductivity and radial temperature gradient. It should be noted that this analysis does not take into account the possible perturbations in the temperature gradient caused by the thermocouple well itself, but only the error due to heat flow down the thermocouple assembly.

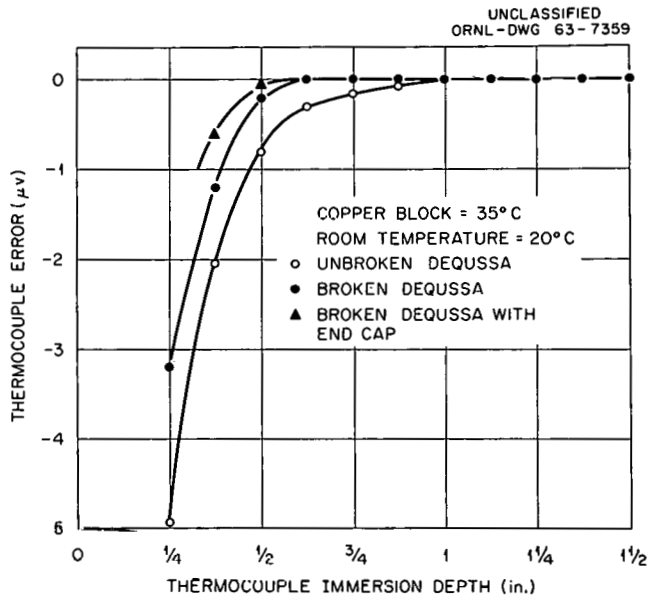

Fig. C.1. Thermocouple Error as a Function of Immersion Depth.

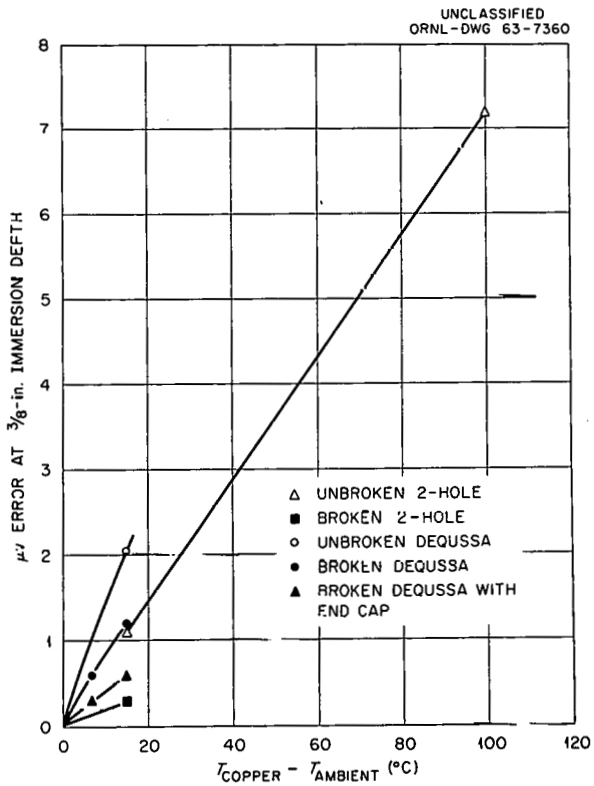

Fig. C.2. Thermocouple Error as a Function of the Temperature Gradient on the Thermocouple for a ⅜-in. Immersion Depth.

Appendix D

UO_2 THERMAL CONDUCTIVITY DATA

Table D.1. Measured Thermal Conductivity Values from Run 1

(Corrected for core-heater expansion)

T (°C)	k, meas (w cm^{-1} $°C^{-1}$)	k_t, corr (w cm^{-1} $°C^{-1}$)	$1/k_t$ (w cm^{-1} $°C^{-1}$)$^{-1}$
55	0.06730	0.07205	13.88
77	0.06605	0.07073	14.13
81	0.06550	0.07012	14.25
91.5	0.06475	0.06932	14.42
107	0.06395	0.06844	14.60
121.5	0.06327	0.06770	14.76
154.5	0.06085	0.06513	15.35
174.5	0.05960	0.06376	15.68
195	0.05820	0.06226	16.06
226	0.05632	0.06024	16.60
259	0.05384	0.05757	17.36
283	0.05234	0.05596	17.87
321	0.05018	0.05362	18.66
348	0.04838	0.05192	19.26
375	0.04723	0.05046	19.81
391	0.04622	0.04938	20.25
424	0.04487	0.04793	20.88
436	0.04456	0.04758	21.02
443	0.04416	0.04715	21.20
473	0.04270	0.04558	21.95
500	0.04204	0.04487	22.30
529	0.04097	0.04372	22.88
559.5	0.03978	0.04246	23.57
584.5	0.03910	0.04168	23.99
609	0.03850	0.04106	24.37
612.5	0.03827	0.04081	24.51
650	0.03699	0.03943	25.37
693	0.03558	0.03792	26.39
739	0.03431	0.03654	27.38
790.5	0.03289	0.03500	28.58
830	0.03192	0.03496	29.43
873	0.03100	0.03297	30.33
601	0.03860	0.04116	24.31
223	0.05935	0.06346	15.76
227	0.05900	0.06310	15.86

Table D.2. Measured Thermal Conductivity Values from Run 2

(Corrected)

T (°C)	k, meas (w cm^{-1} °C^{-1})	k_t, corr (w cm^{-1} °C^{-1})	$1/k_t$ (w cm^{-1} °C^{-1})$^{-1}$
54	0.07400	0.07923	12.62
123	0.06798	0.07273	13.75
189.5	0.06263	0.06699	14.92
301	0.05410	0.05786	17.29
399.5	0.04762	0.05090	19.65
494	0.04336	0.04627	21.62
603.5	0.03918	0.04178	23.94
702.5	0.03577	0.03811	26.25
801	0.03283	0.03496	28.61

Table D.3. Measured Thermal Conductivity Values from Run 3

(Corrected)

T (°C)	k, meas (w cm^{-1} °C^{-1})	k_t, corr (w cm^{-1} °C^{-1})	$1/k_t$ (w cm^{-1} °C^{-1})$^{-1}$
100	0.06722	0.07195	13.89
202	0.05905	0.06317	15.83
402	0.04620	0.04936	20.26
597	0.03810	0.04062	24.63
596	0.03848	0.04103	24.38
607.5	0.03503	0.03733	26.79
798.5	0.03201	0.03407	29.35
892	0.03007	0.03196	31.28
900	0.02997	0.03185	31.39
1006	0.02797	0.02970	33.67
1009	0.02778	0.02950	33.89
1099	0.02658	0.02819	35.45
1192	0.02532	0.02683	37.25

Table D.4. Measured Thermal Conductivity Values from Run 4

(Corrected)

T (°C)	k, meas (w cm^{-1} °C^{-1})	k_t, corr (w cm^{-1} °C^{-1})	$1/k_t$ (w cm^{-1} °C^{-1})$^{-1}$
298.5	0.05196	0.05554	18.00
597	0.03752	0.04001	25.00
597	0.03705	0.03951	25.31
598.5	0.03697	0.03941	25.38
898	0.02909	0.03092	32.32
902	0.02890	0.03073	32.52
1104	0.02617	0.02775	36.02
1201.5	0.02457	0.02601	38.40
1202	0.02407	0.02549	39.18
1298	0.02390	0.02528	39.56

Table D.5. Measured Thermal Conductivity Values from Run 5

(Corrected)

T (°C)	k, meas (w cm^{-1} °C^{-1})	k_t, corr (w cm^{-1} °C^{-1})	$1/k_t$ (w cm^{-1} °C^{-1})$^{-1}$	Bottom Plane Only	
				T (°C)	$1/k_t$ (w cm^{-1} °C^{-1})$^{-1}$
109	0.06497	0.06953	14.38	1052	34.70
110	0.06508	0.06962	14.35	1052	34.31
201	0.05813	0.06216	16.08	1149	36.15
200	0.05763	0.06166	16.01	903	31.10
296.5	0.05147	0.05503	18.09	903	31.27
298.5	0.05120	0.05472	18.13	1052	34.23
400	0.04600	0.04913	20.35	1052	34.41
400	0.04568	0.04879	20.37	1145	36.04
501	0.04090	0.04365	22.90	1224	37.54
501	0.04110	0.04385	22.80	1224	37.82
601.5	0.03726	0.03973	25.17	1272	38.28
601.5	0.03750	0.03998	25.01	1272	38.49
700	0.03432	0.03657	27.34	1351	38.49
700	0.03434	0.03658	27.33	1351	39.25
798	0.03188	0.03393	29.48	1178	35.44
798	0.03183	0.03388	29.52	1076	33.56
900	0.02970	0.03158	31.65	897	29.83
998	0.02773	0.02945	33.95	897	29.84
1050	0.02700	0.02871	34.90	595	23.35
1099	0.02619	0.02776	36.00	296	16.79
1099	0.02615	0.02773	36.02		
1149	0.02543	0.02694	37.07		
1150	0.02530	0.02681	37.26		
1195	0.02481	0.02628	38.01		
1248	0.02417	0.02557	39.10		
1250	0.02433	0.02575	38.92		
1296	0.02339	0.02470	40.45		
1296	0.02334	0.02469	40.56		
1296	0.02317	0.02450	41.00		

Table D.6. Measured Thermal Conductivity Values from Run 6

(Corrected)

T (°C)	k, meas (w cm^{-1} °C^{-1})	k_t, corr (w cm^{-1} °C^{-1})	$1/k_t$ (w cm^{-1} °C^{-1})$^{-1}$
103	0.06802	0.07281	13.73
103	0.06746	0.07221	13.84
303	0.05241	0.05602	17.85
303	0.05238	0.05599	17.86
397.5	0.04702	0.05023	19.91
397.5	0.04701	0.05022	19.91
397.5	0.04707	0.05038	19.89
601	0.03836	0.04091	24.45
50	0.07137	0.07640	13.09

Table D.7. Measured Thermal Conductivity Values from Run 7

(Corrected)

T (°C)	Top Plane with Copper/Constantan Thermocouples			Center Plane with Pt vs Pt–10% Rh Thermocouples		
	k, meas (w cm^{-1} $°C^{-1}$)	k_t, corr (w cm^{-1} $°C^{-1}$)	$1/k_t$ (w cm^{-1} $°C^{-1}$)$^{-1}$	k, meas (w cm^{-1} $°C^{-1}$)	k_t, corr (w cm^{-1} $°C^{-1}$)	$1/k_t$ (w cm^{-1} $°C^{-1}$)$^{-1}$
51	0.07057	0.07555	13.23			
−18	0.06660	0.07130	14.02			
−57	0.06347	0.06795	14.72			
−56	0.06524	0.06985	14.32			
−39	0.06634	0.07102	14.08			
−21	0.06285	0.06729	14.86			
52	0.07111	0.07613	13.13	0.06896	0.07383	13.54
104	0.06651	0.07118	14.04	0.06491	0.06947	14.39
104	0.06656	0.07124	14.03	0.06488	0.06944	14.40
106	0.06692	0.07162	13.96	0.06527	0.06986	14.31
105	0.06533	0.06991	14.30	0.06415	0.06866	14.56
105	0.06528	0.06986	14.31	0.06420	0.06871	14.55
107	0.06534	0.06993	14.29	0.06423	0.06874	14.54
109	0.06687	0.07157	13.97	0.06532	0.06981	14.32

Appendix E

ARMCO IRON THERMAL CONDUCTIVITY AND THERMAL DIFFUSIVITY DATA

Table E.1. Thermal Conductivity Data for Armco Iron

T (°C)	k_{meas} (w cm^{-1} °C^{-1})	k_{corr}[a] (w cm^{-1} °C^{-1})	$k_{corr}-k_{eq.}$ (w cm^{-1} °C^{-1})
		Run 1	
112	0.6577	0.6574	+0.0002
210	0.5963	0.5956	−0.0003
300	0.5324	0.5314	−0.0083
400	0.4818	0.4806	+0.0038
500	0.4256	0.4242	−0.0008
500	0.4245	0.4231	−0.0019
600	0.3803	0.3787	−0.0002
600	0.3806	0.3790	0
698	0.3346	0.3329	−0.0011
698	0.3350	0.3333	−0.0007
717	0.3254	0.3237	−0.0015
717	0.3260	0.3243	−0.0009
741	0.3140	0.3122	−0.0018
741	0.3139	0.3121	−0.0019
780	0.2955	0.2937	−0.0024
780	0.2954	0.2936	−0.0025
819	0.2933	0.2914	−0.0026
		Run 2A	
211	0.6009	0.6002	+0.0050
299	0.5422	0.5412	+0.0011
501	0.4308	0.4294	+0.0049
501	0.4310	0.4296	+0.0051
751	0.3105	0.3087	−0.0007
796	0.2917	0.2899	−0.0031
818	0.2934	0.2915	−0.0021
838	0.2914	0.2895	−0.0047
838	0.2915	0.2896	−0.0046
896	0.2923	0.2902	−0.0057
945	0.2877	0.2855	−0.0025
925	0.2916	0.2895	+0.0038
		Run 2B	
700	0.3398	0.3381	+0.0052
776	0.3011	0.2993	+0.0015
818	0.2950	0.2931	−0.0005
818	0.2953	0.2934	−0.0002
862	0.2967	0.2947	−0.0002
896	0.2967	0.2946	−0.0013
896	0.2972	0.2951	−0.0008
908	0.2976	0.2955	−0.0007
923	0.2859	0.2838	−0.0016
933	0.2872	0.2851	−0.0015
		Run 2C	
933	0.2902	0.2881	+0.0015
969	0.2948	0.2925	+0.0016
1000	0.2962	0.2938	−0.0009
		Run 2D	
752	0.3147	0.3129	+0.0041
752	0.3146	0.3128	+0.0040
849	0.2980	0.2960	+0.0015
898	0.3003	0.2982	+0.0023
925	0.2888	0.2867	+0.0010

[a]Corrected for core-heater expansion.

Table E.2. Comparison of Other Measurements with ORNL Equations

Temperature (°C)	Thermal Conductivity (w cm^{-1} $°C^{-1}$)								
	A ORNL	B Powell (BMI Iron)	B − A	C Powell (Most Probable)	C − A	D Laubitz (BMI Iron)	D − A	E Cody, Abeles, and Beers[a]	E − A
0	0.7273	0.747	+0.0197	0.749	+0.0277				
30	0.7085					0.691	−0.0175		
100	0.6647	0.686	+0.0213	0.672	+0.0073	0.647	−0.0177	0.6600	−0.0047
200	0.6021	0.621	+0.0189	0.608	+0.0059	0.584	−0.0181	0.6103	+0.0082
300	0.5395	0.555	+0.0155	0.548	+0.0085	0.528	−0.0115	0.5561	+0.0166
400	0.4769	0.492	+0.0151	0.487	+0.0101	0.474	−0.0029	0.4932	+0.0163
500	0.4249	0.430	+0.0051	0.433	+0.0081	0.427	+0.0021	0.4290	+0.0041
600	0.3788	0.382	+0.0032	0.389	+0.0102	0.383	+0.0042	0.3696	−0.0092
700	0.3328	0.339	+0.0062	0.345	+0.0122	0.340	+0.0072	0.3190	−0.0138
800	0.2936	0.294	+0.0004	0.300	+0.0064	0.305	+0.0114	0.2982	+0.0046
900	0.2956	0.282	−0.0136	0.286	−0.0096	0.291	−0.0046	0.3056	+0.0100
950	0.2886	0.287	−0.0016	0.289[b]	+0.0004	0.300[b]	+0.0114	0.2892	+0.0006
1000	0.2948	0.293	−0.0018	0.292	−0.0028	0.303	+0.0082	0.2907	−0.0041

[a]Calculated from diffusivity values read from curve and McElroy's specific heat data.

[b]Read from graphs by Powell and Laubitz.

Table E.3. Thermal Diffusivity Data of Cody, Abeles, and Beers[38] Compared to Values Calculated from ORNL Data and McElroy's[39] Specific Heat Values

Temperature (°C)	$k_{eq.}$ (w cm^{-1} $°C^{-1}$)	c_P (wsec g^{-1} $°C^{-1}$)	$\alpha = \frac{k}{c_P \rho^{*a}}$ (cm^2/sec)	Temperature (°C)	α, Cody, Abeles, and Beers (cm^2/sec)
100	0.6647	0.4813	0.1761	80	0.196
200	0.6021	0.5245	0.1471	150	0.157
300	0.5395	0.5660	0.1227	270	0.132
400	0.4769	0.6098	0.1012	350	0.110
500	0.4249	0.6638	0.0832	440	0.096
600	0.3788	0.7446	0.0664	550	0.078
700	0.3328	0.9260	0.0471	555	0.075
720	0.3238	0.9920	0.0428	620	0.064
730	0.3191	1.029	0.0408	660	0.057
750	0.3099	1.267	0.0362	720	0.045
760	0.3054	1.229	0.0327	740	0.041
780	0.2961	0.9852	0.0396	740	0.040
800	0.2936	0.8860	0.0437	760	0.033
820	0.2940	0.8386	0.0462	775	0.040
850	0.2947	0.7934	0.0491	790	0.043
900	0.2956	0.7516	0.0520	800	0.044
925	0.2857	0.6222	0.0601	820	0.047
950	0.2886	0.6264	0.0604	845	0.049
1000	0.2948	0.6347	0.0610	860	0.049
				900	0.054
				900	0.053
				920	0.062
				920	0.060
				950	0.061
				950	0.060
				1000	0.061

[a] $\rho^* = \rho_0^* (1 - 3\alpha_L t)$; α_L obtained from *Metals Handbook*, vol 1, 8th Ed. p 1207.
$\rho_0^* = 7.874$ g/cm^3.

Table E.4. Lattice Electronic Portion of Thermal Conductivity of Armco Iron Obtained by Two Methods and Resulting Lattice Thermal Conductivity

Temperature (°C)	Conductivity, k_L (w cm^{-1} $°C^{-1}$)	
	From Backlund and Linde[a]	From Wiedemann-Franz-Lorenz[b]
100	0.174	0.094
150	0.166	0.104
200	0.158	0.109
250	0.150	0.110
300	0.142	0.110
350	0.133	0.108
400	0.124	0.102
450	0.114	0.097
500	0.108	0.094
550	0.101	0.089
600	0.093	0.083
650	0.084	0.077
700	0.076	0.070
750	0.067	0.063
800	0.056	0.053
850	0.055	0.050
900	0.049	0.045
910	0.046	0.044
920	0.037	0.032
950	0.035	0.031
1000	0.032	0.030

[a] $\left(k_L = k - \frac{LT}{\rho + 2.66}\right)$; k_L from Backlund and Linde, and k from ORNL equations.

[b] $\left(k_L = k - \frac{LT}{\rho}\right)$; k_L from Wiedemann-Franz-Lorenz, and k from ORNL equations.

Appendix F

DETERMINATE ERRORS IN ELECTRICAL RESISTIVITY MEASUREMENTS

Equation (21), used to calculate the electrical resistivity of Armco iron, can be differentiated to give an expression for the fractional error in $\rho(\Delta\rho/\rho)$ due to errors in the terms of the equation, and this yields

$$\left|\frac{\Delta\rho}{\rho}\right|_{max} = \left|\frac{\Delta(\Delta\bar{V})}{\Delta\bar{V}}\right| + \left|\frac{\Delta A^*}{A^*}\right| + \left|\frac{\Delta L^*}{L^*}\right| + \left|\frac{\Delta\bar{I}}{\bar{I}}\right|,$$

if one ignores the uncertainty in the expansion coefficient, α. The error in the potentiometer reading, $\Delta\bar{V}$, depended on the range used in the measurement, but the maximum value was about $\pm 0.02\%$. The same error is involved in the current measurement along with about a 0.05% uncertainty in the resistance of the standard resistor. The specimen was ground to a diameter of 0.1000 ± 0.0001 in. as measured by a micrometer so that the uncertainty in A^*, ΔA^*, was 0.2% since the diameter is squared. The error in the length between Pt–10% Rh legs was no greater than twice the diameter of the wire, or 2×0.005 in. This length was measured by a traveling stage microscope. Thus the error in the length was about 1%. Adding these contributions yields a $|\Delta\rho/\rho|_{max}$ of about 1.3%, which is reduced to 1.0% if the various contributions are random.

Appendix G

ELECTRICAL RESISTIVITY DATA FOR ARMCO IRON

Table G.1. Measured Electrical Resistivity Values for Armco Iron and Calculated Electronic Portion of Thermal Conductivity

Temperature (°C)	Temperature (°K)	ρ (μohm-cm)	$k_e = \frac{LT}{\rho}$ (w cm^{-1} °C^{-1})	$k_c = \frac{LT}{\rho + 2.66}$ (w cm^{-1} °C^{-1})
99.8		16.3[a]		
205.0		24.3[a]		
311.8		34.3[a]		
314.4		34.6[a]		
618.2		75.2[a]		
−196.0	77.2	1.92[b]	0.982	0.413
−78.9	194.3	6.43[b]	0.741	0.523
0	273.2	10.19[b]	0.658	0.519
18.3	291.5	11.08	0.644	0.518
23.0	296.2	11.40[b]	0.637	0.515
103.7	376.9	16.2	0.570	0.488
107.4	380.6	16.4	0.568	0.488
201.8	475.0	23.6	0.493	0.442
227.8	501.0	25.7	0.478	0.431
276.5	549.7	30.4	0.443	0.407
307.7	580.9	33.5	0.425	0.393
350.8	624.0	38.2	0.400	0.374
378.2	651.4	41.1	0.388	0.365
401.1	674.3	44.0	0.375	0.354
422.0	695.2	46.6	0.365	0.345
446.5	719.7	49.8	0.354	0.336
485.9	759.1	54.9	0.338	0.323
507.8	781.0	58.1	0.329	0.315
542.8	815.9	63.1	0.317	0.307
581.6	854.8	69.1	0.303	0.292
672.8	946.0	85.1	0.273	0.264
703.8	977.0	91.1	0.263	0.255
744.6	1017.8	99.3	0.251	0.244
752.8	1026.0	102.2	0.246	0.240
776.8	1050.0	106.3	0.242	0.236
797.3	1070.5	108.4	0.242	0.237
798.2	1071.4	108.6	0.241	0.236
807.7	1080.9	109.3	0.244	0.238
847.0	1120.2	112.2	0.244	0.238
896.9	1170.1	114.3	0.251	0.245
918.8	1192.0	115.1	0.253	0.247
951.5	1224.7	116.2	0.258	0.252
991.4	1264.6	117.5	0.264	0.257
996.4	1269.6	117.4	0.265	0.260

[a] Results obtained prior to 620°C anneal.

[b] Results obtained in different apparatus on same specimen.

Appendix H

ELECTRICAL RESISTIVITY DATA OF Pt vs Pt–10% Rh

Table H.1. Measured Electrical Resistance and Calculated Electrical Resistivity

Temperature (°C)	Core-Heater Resistance (ohms)	Calculated Resistivity[a] of Pt–10% Rh Core Heater (μohm-cm)
23.5	0.3704	19.20
95	0.4131	21.41
210	0.4800	24.88
299	0.5300	27.48
400	0.5845	30.30
500	0.6382	33.09
600	0.6913	35.81
698	0.7410	38.40
741	0.7624	39.51
780	0.7819	40.51
211	0.4812	24.95
500	0.6398	33.14
751	0.7680	39.80
795	0.7892	40.90
818	0.8004	41.49
838	0.8097	41.95
896	0.8372	43.39
945	0.8606	44.60
925	0.8514	44.11
700	0.7433	38.51

[a] $\rho = \Omega A^*/L^*$; $L^* = 30.75$ in.; $A^* = \pi d^2/4$; $d = 0.0508$ cm.

Appendix I

SAMPLE DATA SHEETS AND CALCULATIONS

All data were recorded on sheets similar to those of Figs. I.1 and I.2. The letters *I* and *O* designate thermocouples located at the inside (r_1) and outside (r_2) radii, respectively, while the small hyphenated numbers refer to the thermocouple switching circuitry.

Sheet No.: 36 Sample: Armco Date: 8-9-63

ISOTHERMAL Operator: J.P.M. Time: 3:00 PM

1-1	Top Plane	Bottom Plane	Muffle Control	Inside Control	Guard Control
I_1	2-1 5233.97	2-7 5231.97	7-6 T 4582.0	1-4 T 5234.48	7-5 T 5173.34
I_2	2-2 5233.23	2-8 5234.43	1-7 C 5127.4	1-5 C 5232.07	7-2 B 5195.57
I_3	2-3 5232.36	2-9 5232.76	7-1 B 4606.0	1-6 B 5234.43	
Av	5233.18	5233.05		Av 5232.98 μv	νμ

O_1	2-4 5232.61	2-10 5233.01	Center Plane
O_2	2-5 5233.12	2-11 5233.07	7-3 I
O_3	2-6 5232.13	2-12 5233.18	7-4 O
Av	5232.62	5233.09	

Temperature 600°C

Sensitivity

K-3
Voltage (←)9

K-3
Current (←)10

Power

Av Diff.	+0.56	-0.04	
TC Corr.	-0.56	+0.04	
Corr. Diff.			
X			
XVIS			
K			

VIS

$K = \frac{XVIS}{\Delta E}$

Fig. I.1. Sample "Isothermal" Data Sheet for Armco Iron at 600°C.

Figure I.1 shows a set of Armco iron data taken under isothermal conditions at 600°C. The twelve thermocouple emf's of the two measuring planes were read directly, the readings were properly averaged, and the average differences between the inside and outside positions were

Sheet No.: 38 Sample: Armco Date: 8-12-63

DATA Operator: G Time: 4:15 PM

1-1	Top Plane	Bottom Plane	Muffle Control	Inside Control	Guard Control
I_1	2-1 5252.20	2-7 5247.10	7-6 T 4395.0	1-4 T 5227.46	7-5 T 5277.3
I_2	2-2 51.73	2-8 52.61	1-7 C 4855.6	1-5 C 5227.50	7-2 B 5355.2
I_3	2-3 50.60	2-9 50.38	7-1 B 4393.0	1-6 B 5227.59	
Av	5251.51	5250.03			

Av 5235.30 μv

O_1	2-4 5220.03	2-10 5218.28	Center Plane
O_2	2-5 21.34	2-11 20.68	7-3 I
O_3	2-6 19.67	2-12 19.04	7-4 O
Av	5220.35	5219.33	

Av Diff.	31.16	30.70	
TC Corr.	-0.56	+0.04	
Corr. Diff.	30.60	30.74	

X	0.020155	0.020154	
XVIS	1.1664156	1.1663577	

K	0.38118	0.37943	

Temperature

Sensitivity 10.196

Voltage K-3 6.3835
(←)9 6.3837

Current K-3 8.8914
(←)10 8.8916

Power 56.7598

VIS 57.87227

$K = \frac{XVIS}{\Delta E}$

$0.38030 = \bar{k}_{meas} = \bar{k}_m$

$k_{true} = \bar{k}_m (1 - \alpha T)$

$= 0.38030 (0.9958)$

$= 0.37870$

Fig. I.2. Sample Data Sheet for Armco Iron at 600°C.

recorded. These numbers are the so-called isothermal corrections. It should be noted that in the case of Armco iron the differential emf's were obtained only from absolute measurements rather than from both direct differential emf and absolute emf measurements as in the case of UO_2 It was observed during the course of measurements on UO_2 that the agreement between the differences calculated and those measured directly was always within 0.02 μv and, most often, 0.01 μv. This agreement, together with the fact that differential emf measurements at temperatures above 600°C were hindered by the apparent high-resistance shorting of the differential thermocouple junctions, prompted the adoption of this simplified data-acquisition procedure.

Figure I.2 shows the companion set of data on Armco iron taken with power applied to the core heater and the controllers reset to give the same average specimen temperature. The dc voltage and current were measured both before and after the thermocouple emf's were determined, and the averages were used to calculate the power dissipated by the 3-in. center section of the core heater. The averages of the groups of thermocouples were calculated, and from these, the average differences. The previously determined isothermal corrections (Fig. I.1) were algebraically applied to yield the corrected differentials. The thermocouple sensitivity at the average specimen temperature was obtained from the computer-generated set of tables described in the text. Since the ΔT was so small in these experiments, the error introduced by the use of the sensitivity corresponding to the average temperature is less than 0.01%. The "X" appearing in the table and in the equation for k is unique to the particular specimen and is equal to $\ln (r_2/r_1)/2\pi L$. The radii to the centers of the holes in the Armco specimen and the calculations yielding the "X" values are:

	Top Plane (in.)	Bottom Plane (in.)
I_1	0.4999	0.5001
I_2	0.5002	0.5000
I_3	0.5001	0.5002
I_{av}	0.5001	0.5001
$\ln I_{av}$	-0.6929472	$-0.6929472 = \ln r_1$
O_1	1.3124	1.3126
O_2	1.3126	1.3125
O_3	1.3126	1.3127
O_{av}	1.3125	1.3126
$\ln O_{av}$	0.2719337	$0.2720099 = \ln r_2$
$\ln r_2 - \ln r_1$	0.9648809	$0.9649571 = \ln r_2/r_1$
L	3.00 in. × 2.54 cm/in.	
$\frac{\ln r_2/r_1}{2\pi L}$	0.020153	$0.020154 = X$

It may be noted that the logarithms of the average radii are taken rather than the average of the logarithms of the radii. It is not clear exactly which average should be used, but the difference is only 1 ppm and is therefore insignificant.

The thermal conductivity, k, uncorrected for the thermal expansion of the core heater, is calculated using the tabulated data for each of the separate planes, and the average k is then obtained. This average k is corrected for the expansion of the core heater by the relation

$$k_{\text{true}} = k_{\text{measured}} (1 - \alpha T) ,$$

where α is the coefficient of thermal expansion of Coors AD-99 Al_2O_3, and T is the core-heater temperature. As a matter of convenience, all of the results were corrected after the conclusion of the experiment through the use of correction charts and graphs.

This sample calculation represents the result shown on line 7, run 1, of Table E.1.

THIS PAGE

WAS INTENTIONALLY

LEFT BLANK

ORNL-3556
UC-25 – Metals, Ceramics, and Materials
TID-4500 (29th ed.)

INTERNAL DISTRIBUTION

1. Biology Library
2. Reactor Division Library
3-5. Central Research Library
6-7. ORNL – Y-12 Technical Library Document Reference Section
8-201. Laboratory Records Department
202. Laboratory Records, ORNL R.C.
203. R. E. Adams
204. C. D. Baumann
205. R. J. Beaver
206. C. Brandon
207. N. H. Briggs
208. W. H. Cook
209. J. W. Cooke
210. J. H. Crawford
211. J. E. Cunningham
212. P. B. Denee
213. W. S. Ernst, Jr.
214. J. I. Federer
215. J. H Frye, Jr.
216. W. Fulkerson
217. H. W. Godbee
218. T. G. Godfrey
219. W. O. Harms
220-224. M. R. Hill
225. G. W. Keilholtz
226. T. G. Kollie
227. C. E. Larson
228. G. H. Llewellyn
229. H. G. MacPherson
230-259. D. L. McElroy
260. C. J. McHargue
261. H. A. McLain
262. J. P. Moore
263-264. R. B. Parker
265. S. A. Rabin
266. M. W. Rosenthal
267. G. Samuels
268. O. Sisman
269. M. J. Skinner
270. J. A. Swartout
271. W. C. Thurber
272-292. D. B. Trauger
293. G. M. Watson
294. A. M. Weinberg
295. W. J. Werner
296. G. C. Williams
297. A. A. Burr (consultant)
298. J. R. Johnson (consultant)
299. C. S. Smith (consultant)
300. R. Smoluchowski (consultant

EXTERNAL DISTRIBUTION

301. Research and Development Division, ORO
302. C. M. Adams, Jr., Massachusetts Institute of Technology
303-304. David F. Cope, Oak Ridge Operations
305-306. General Electric, Hanford (1 copy each to D. E. Baker and Ersel Evans)
307. J. L. Gregg, Cornell University
308-309. AEC, Washington (1 copy each to J. Simons and Donald K. Stevens)
310. E. E. Stansbury, University of Tennessee
311. Lawrence M. Slifkin, University of North Carolina
312-885. Given distribution as shown in TID-4500 (29th ed.) under Metals, Ceramics, and Materials category (75 copies – OTS)